Tropical Clouds Life Cycles, Organization and Cloud Processes: Potential Impact of Aerosol
Part B

Luiz A. T. Machado
Luiz.machado@inpe.br
INPE-CPTEC

Gravity Waves on the cloud top

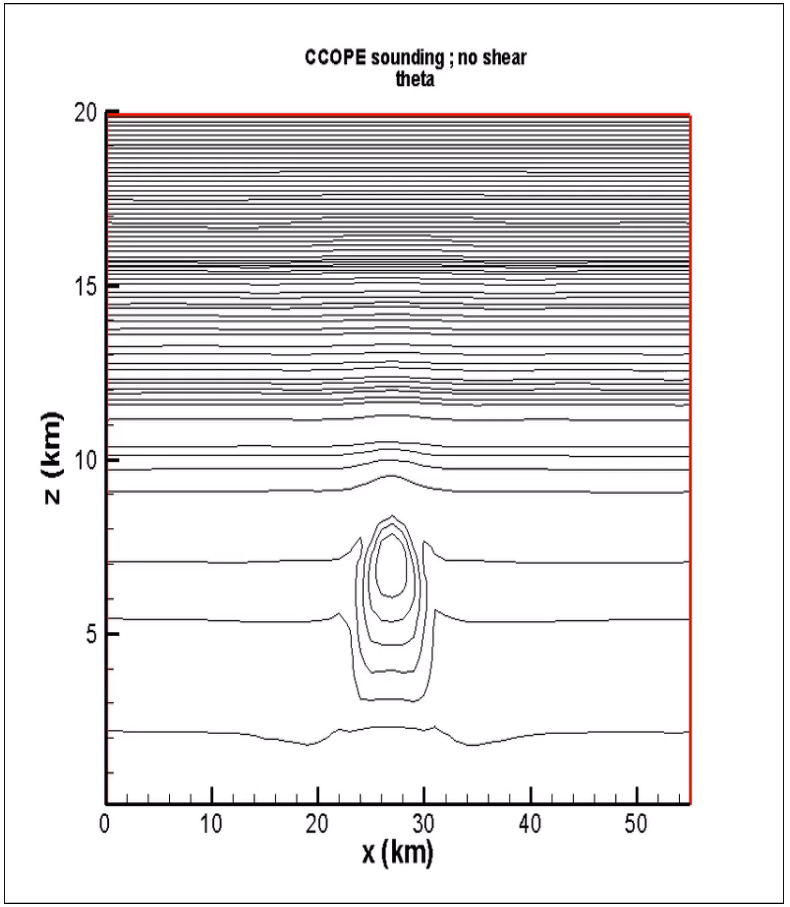

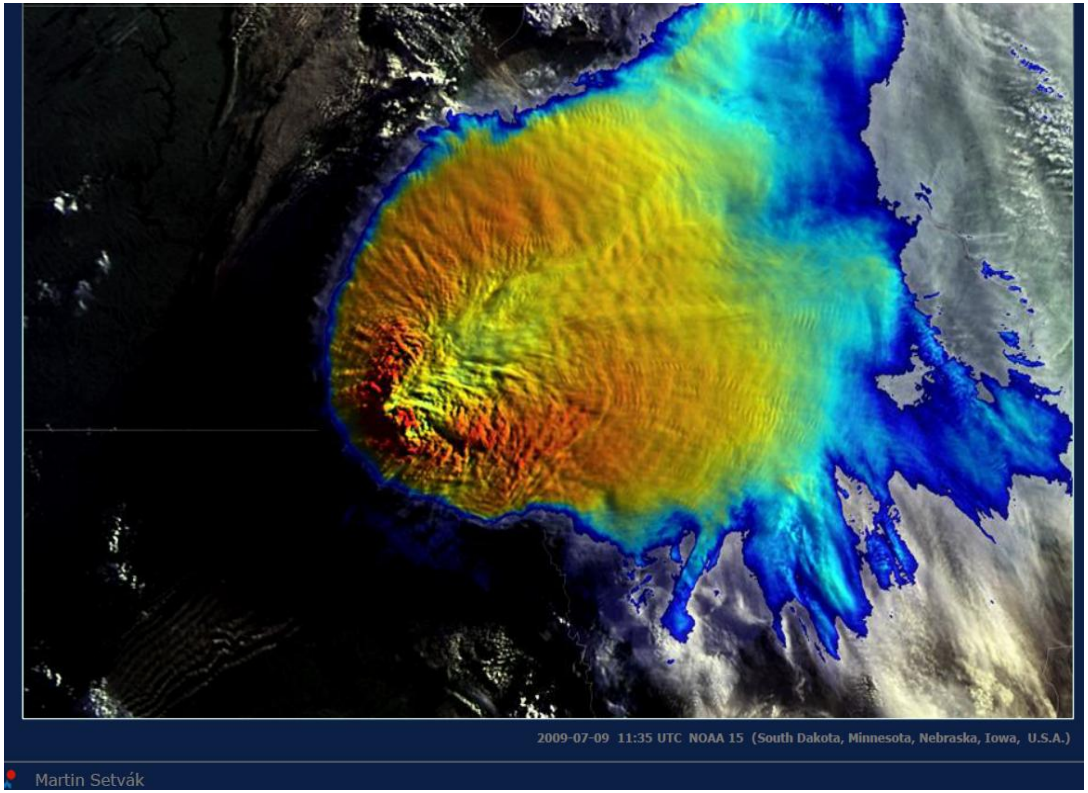
2009-07-09 11:35 UTC NOAA 15 (South Dakota, Minnesota, Nebraska, Iowa, U.S.A.)
Martin Setvák

TB (K) – Channel 9 MSG (10.8 μm)

03/08/2006
14:30UTC

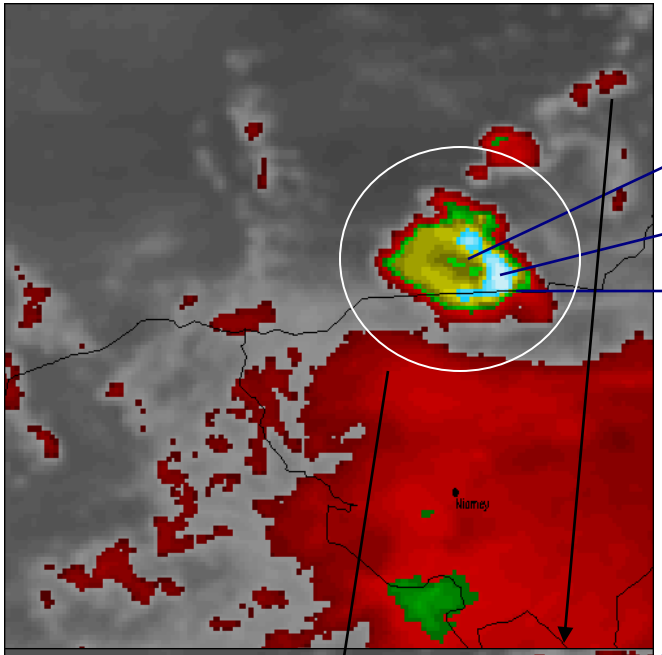

Warmer Region = 200 K

The Coldest Pixel = 189 K

U/V Shape colder region

03/08/2006
17:00UTC

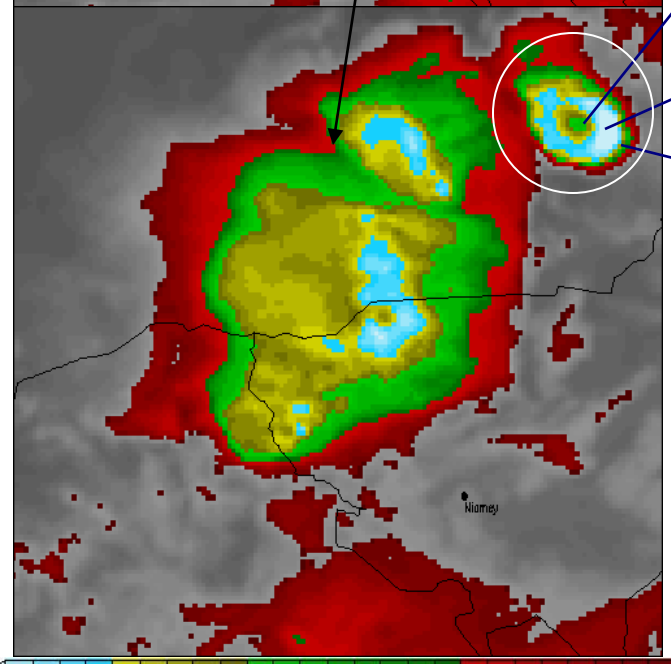

Warmer Region = 200 K

The Coldest pixel = 189 K

Ring Shape – Colder region

V- SHAPED

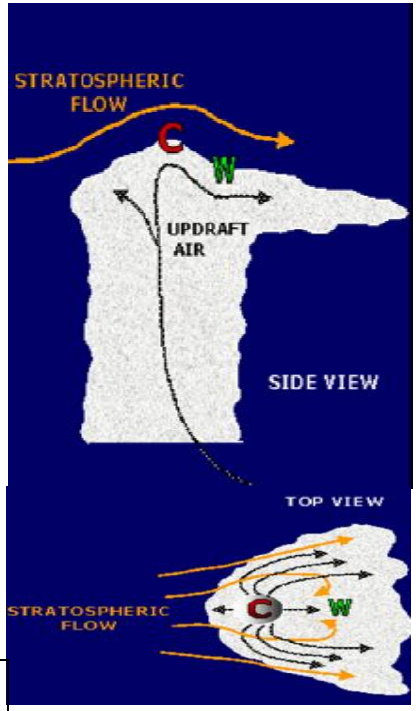

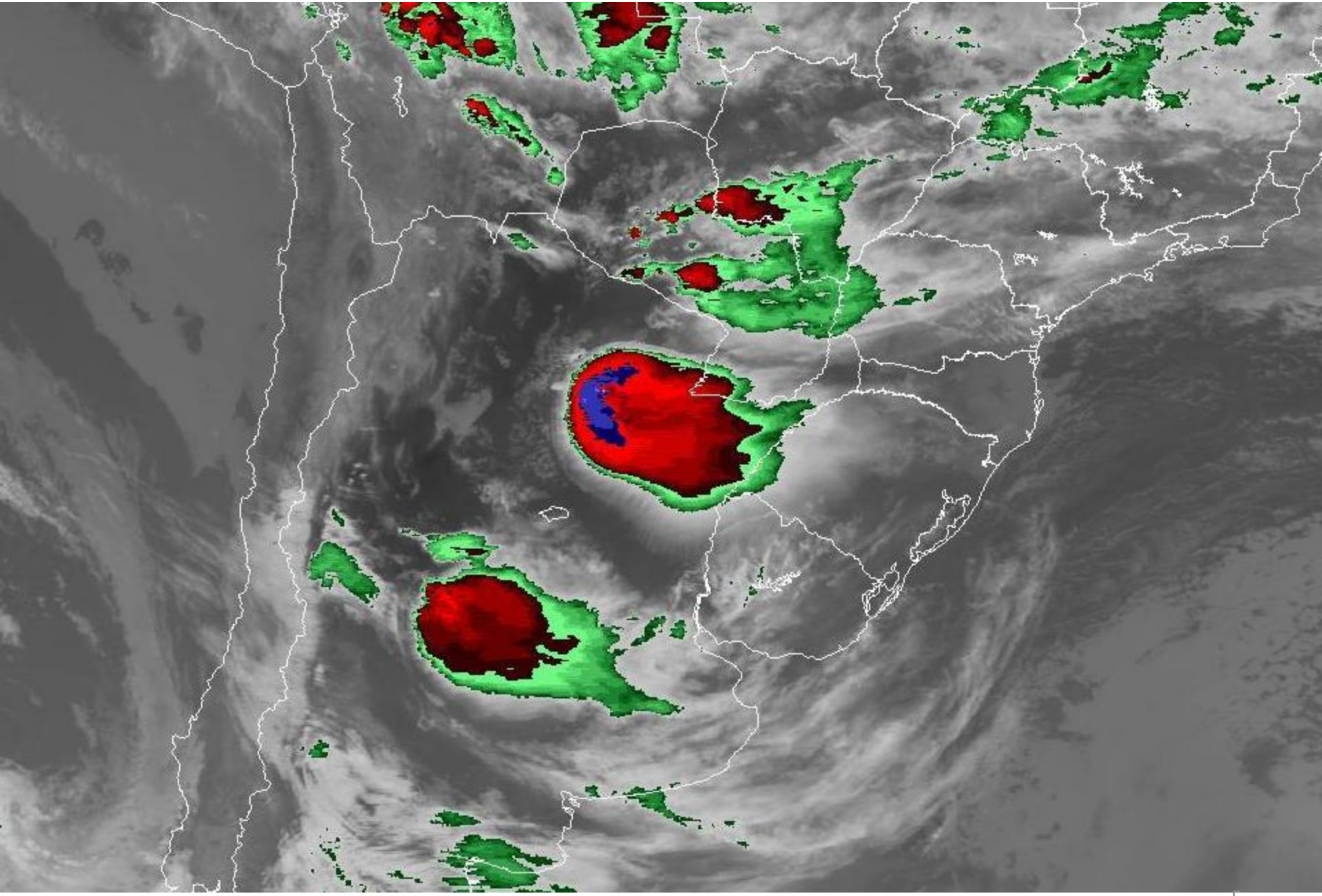

Cold-V, CWA, warm-cold couplet, distant warm area

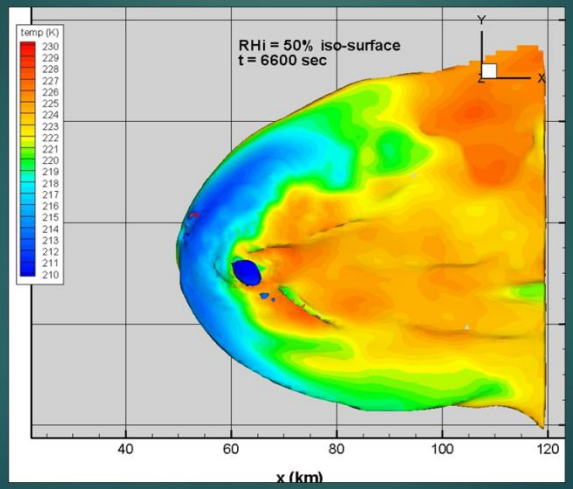

Interaction between ambient wind and updraft

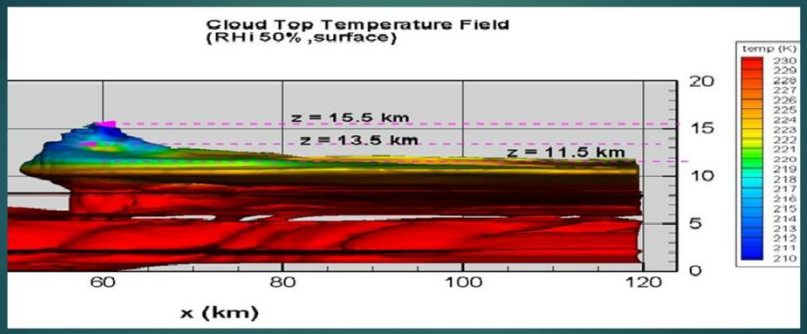

Above anvil cirrus plumes

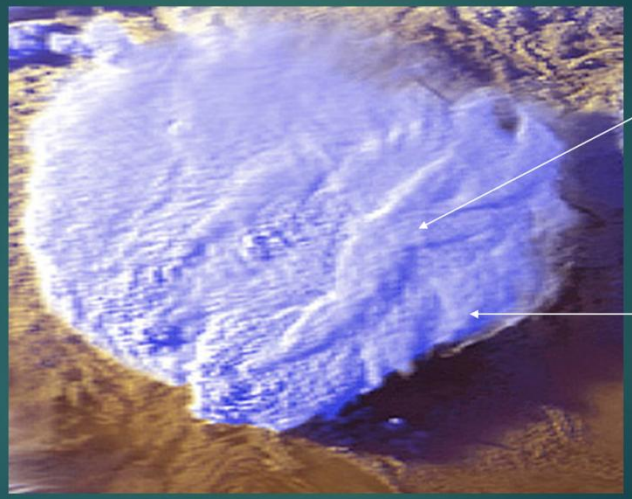

Storms over Balearic Islands

Courtesy Paul Wang

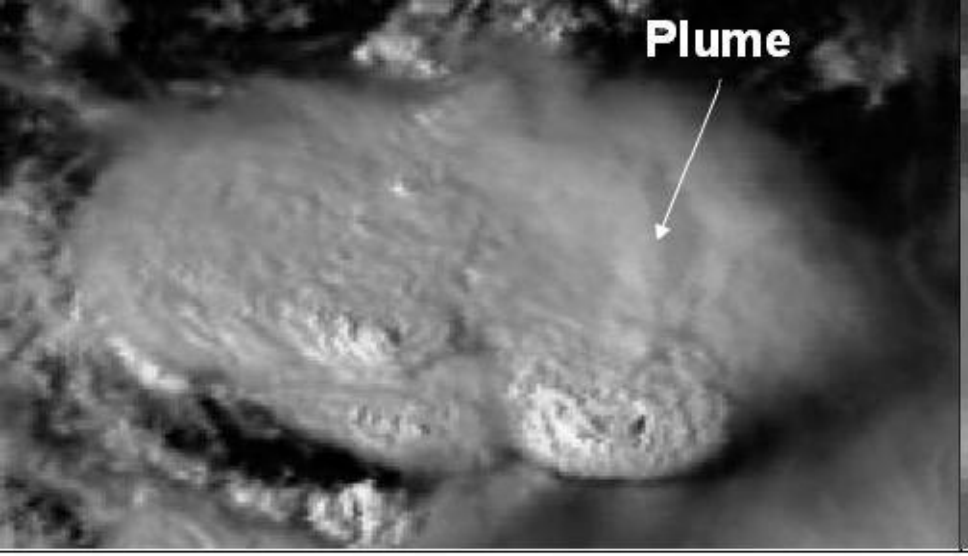

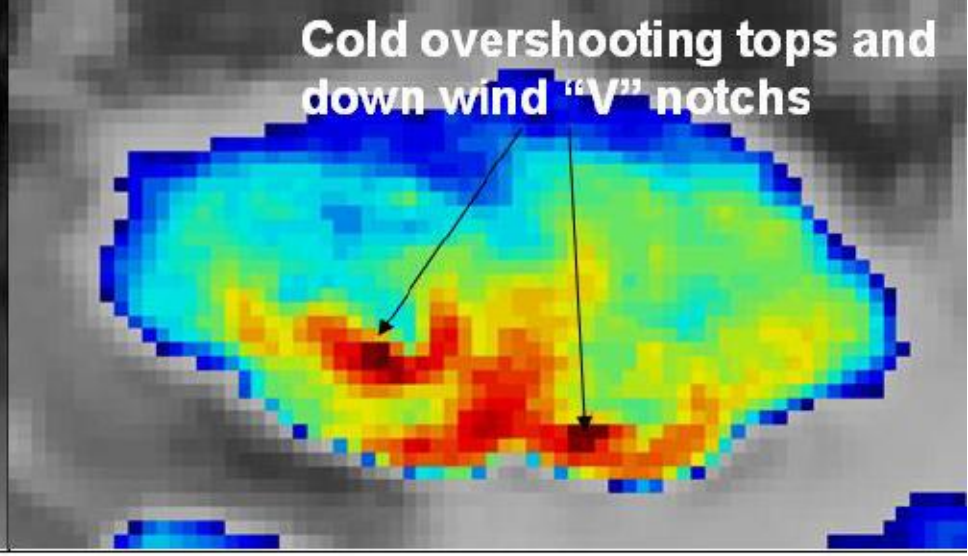

MSG High Resolution Visible (HRV)

MSG Enhanced 10.7 micron IR

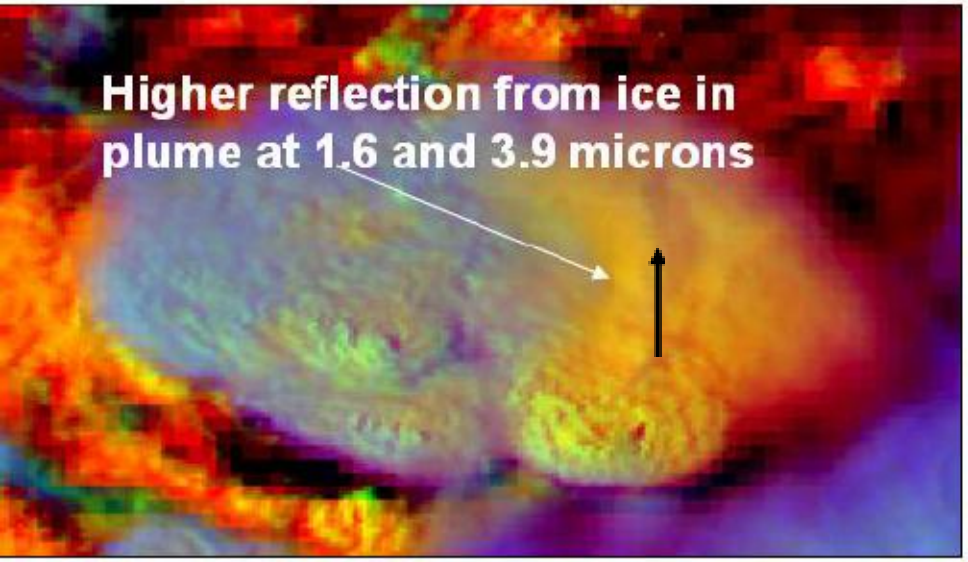

MSG 3 channel color image using HRV, 1.6 and 3.9 micron channel data

Figure 27: Thunderstorm tops over Europe from MSG on 29 July 2005 at 14:30 UTC. This case, presented by Martin Sevtak at the EUMETSAT Users' Conference showed higher reflection from ice in the plume at thunderstorm top in 1.6 and 3.9 microns, likely due to smaller cloud particle size and related to updraft characteristics. Cold over-shooting top and "V" notches are clearly shown in the 10.7 channel image, as are the plume brighter reflection from the right-most storm.

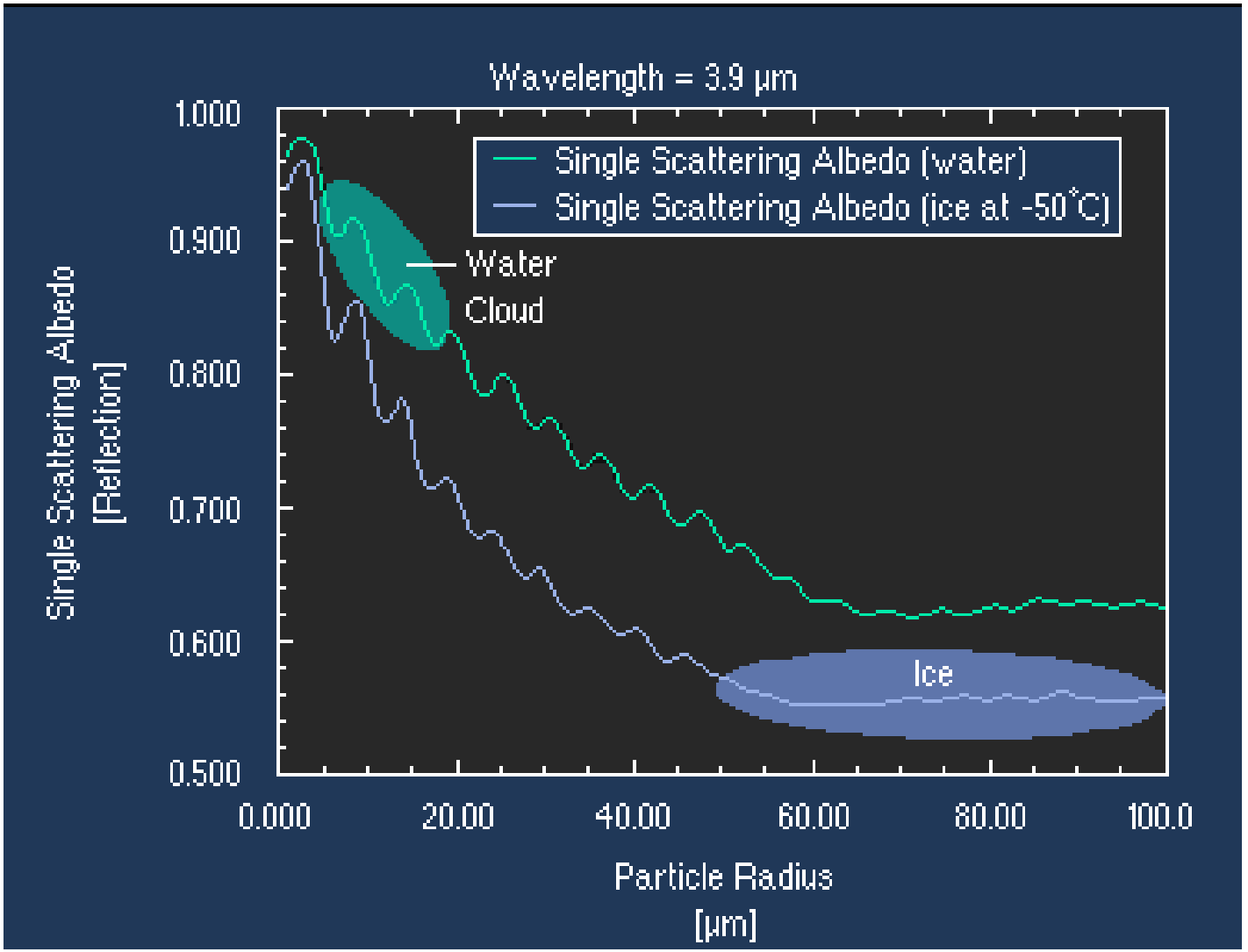
Wavelength = 3.9 μm
Single Scattering Albedo (water)
Single Scattering Albedo (ice at -50°C)
Water Cloud
Ice
Single Scattering Albedo [Reflection]
1.000
0.900
0.800
0.700
0.600
0.500
0.000
20.00
40.00
60.00
80.00
100.0
Particle Radius [μm]

• Raio efetivo da gota de nuvens com Canal 4

D. Rosenfeld, G. Gutman / Atmospheric Research 34 (1994) 259–283

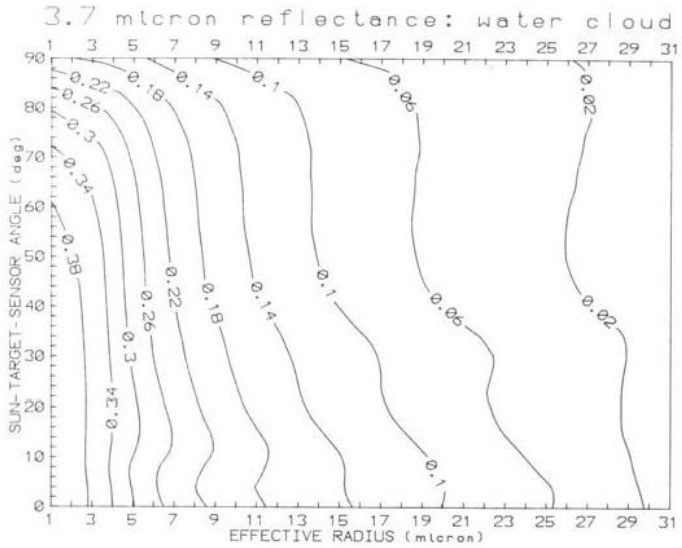

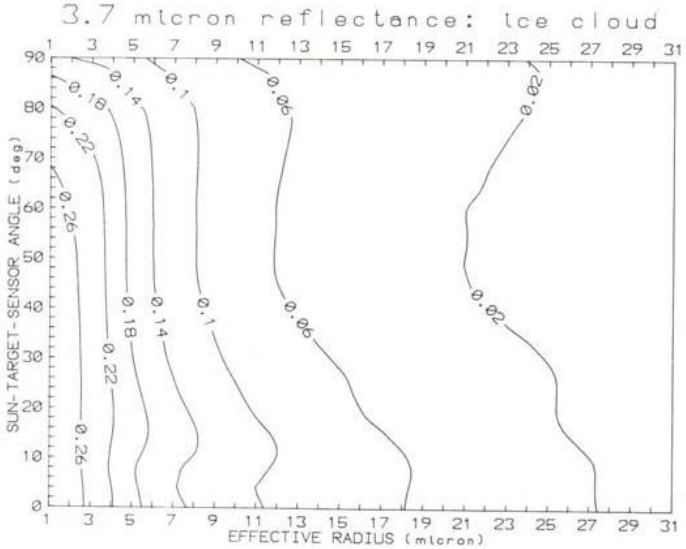

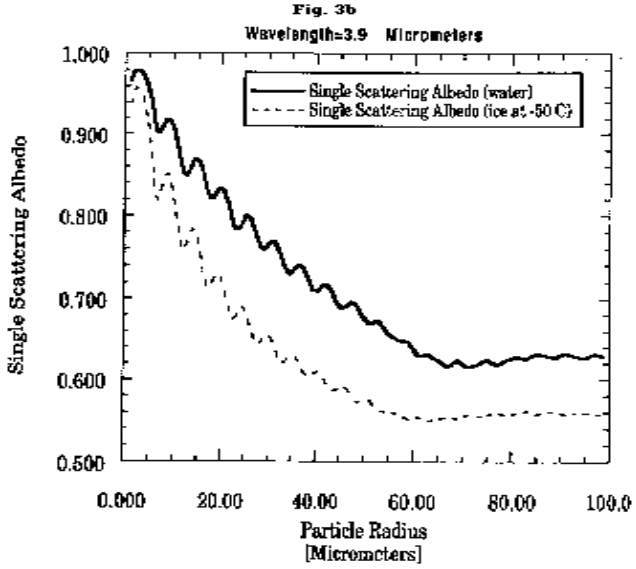

IR3.9 shows much more cloud top structures than IR10.8 (very sensitive to particle size)

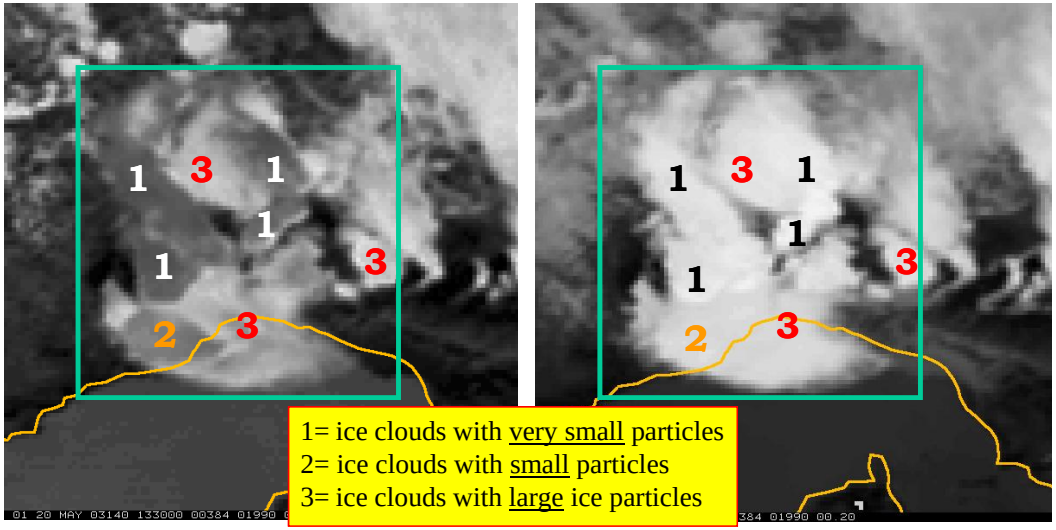

Channel 04 (IR3.9) Channel 09 (IR10.8)

MSG-1, 20 May 2003, 13:30 UTC

SATCAST CI Interest Fields: Original Usage With Critical Value Thresholds

Cloud-top Glaciation

Cloud-top growth

Cloud height, relative to mid-troposphere (Ackerman, 1996; Schmetz et al, 1997)

Cloud height (Inoue, 1997; Prata, 1989; Ellrod, 2004)

Cloud-top height changes

CI interest field	Critical value	
10.7-μm T_B (one score)	<0°C	1
10.7-μm T_B time trend (two scores)	<-4°C $(15\ \text{min})^{-1}$	2
	ΔT_B $(30\ \text{min})^{-1} < \Delta T_B$ $(15\ \text{min})^{-1}$	
Timing of 10.7-μm T_B drop below 0°C (one score)	Within prior 30 min	
6.5 (or 6.7)–10.7-μm difference (one score)	$-35°$ to -10°C	3
13.3–10.7-μm difference (one score)	$-25°$ to -5°C	4
12.0–10.7-μm difference	$-3°$ to 0°C (*GOES-11*)	
6.5 (or 6.7)–10.7-μm time trend (one score)	$>3°$ $(15\ \text{min})^{-1}$	5
13.3–10.7-μm time trend (one score)	$>3°$ $(15\ \text{min})^{-1}$	6
12.0–10.7-μm time trend	$>2°$ $(5\ \text{min})^{-1}$ (*GOES-11*)	

Table from Mecikalski and Bedka (2006)

Cloud top Signature

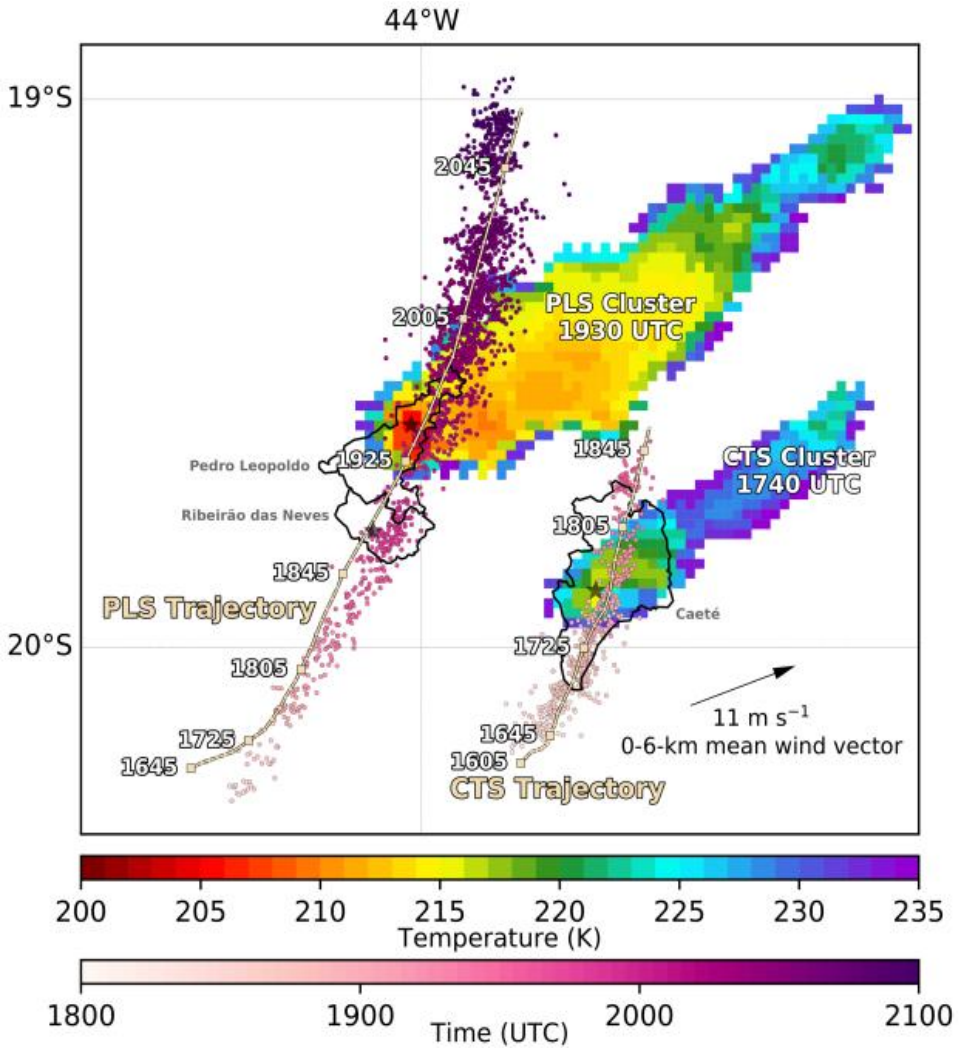

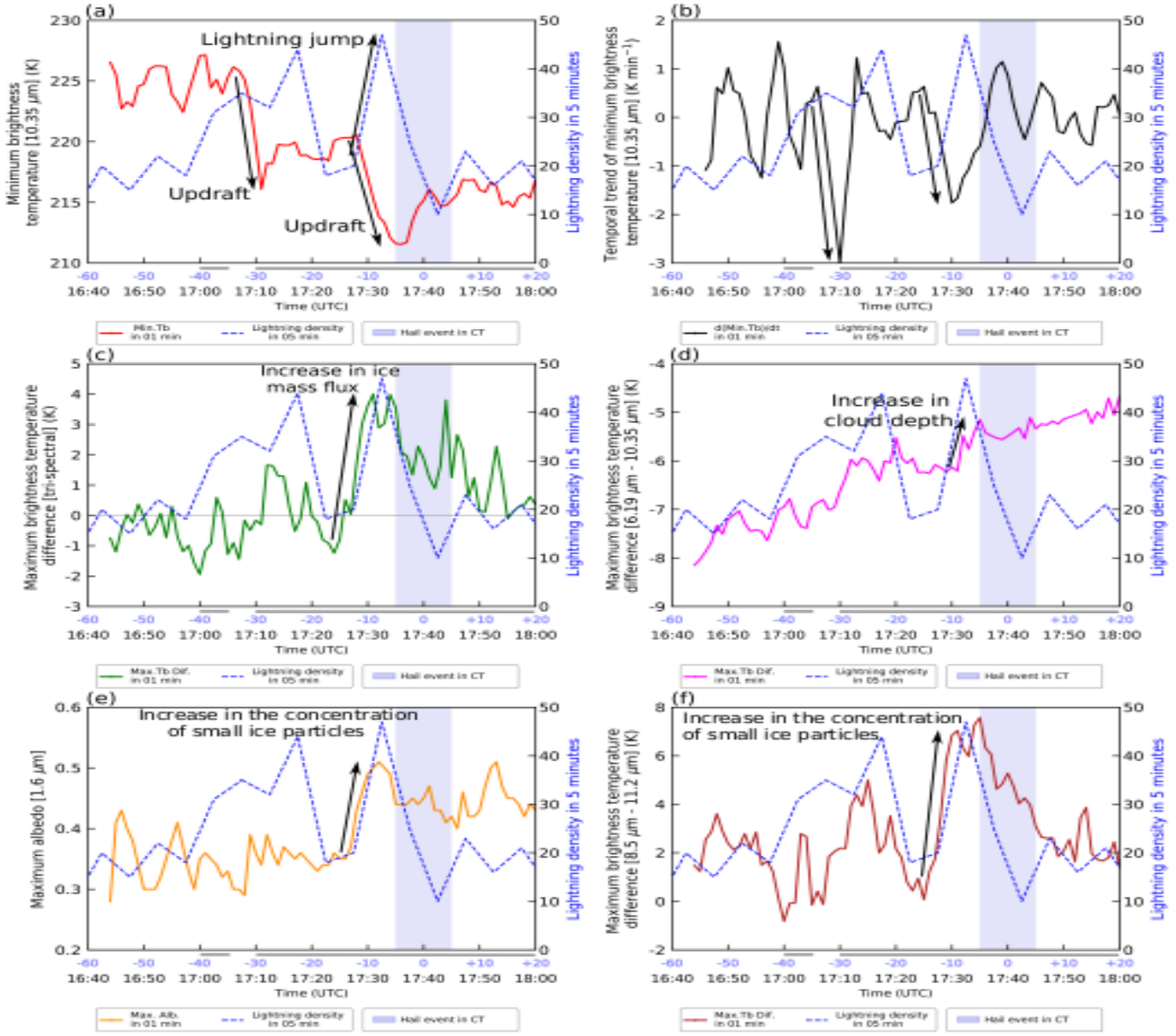

Bruno Z. Ribeiro[1] Luiz A. T. Machado, Joao H. Huamán Ch, Thiago S. Biscaro, Edmilson D. Freitas[2], Kathryn W. Mozer[3] and Steven J. Goodman. An Evaluation of the GOES-16 Rapid Scan for Nowcasting in Southeastern Brazil: Analysis of a Severe Hailstorm Case, Submitted to Weather and Forecasting 2019

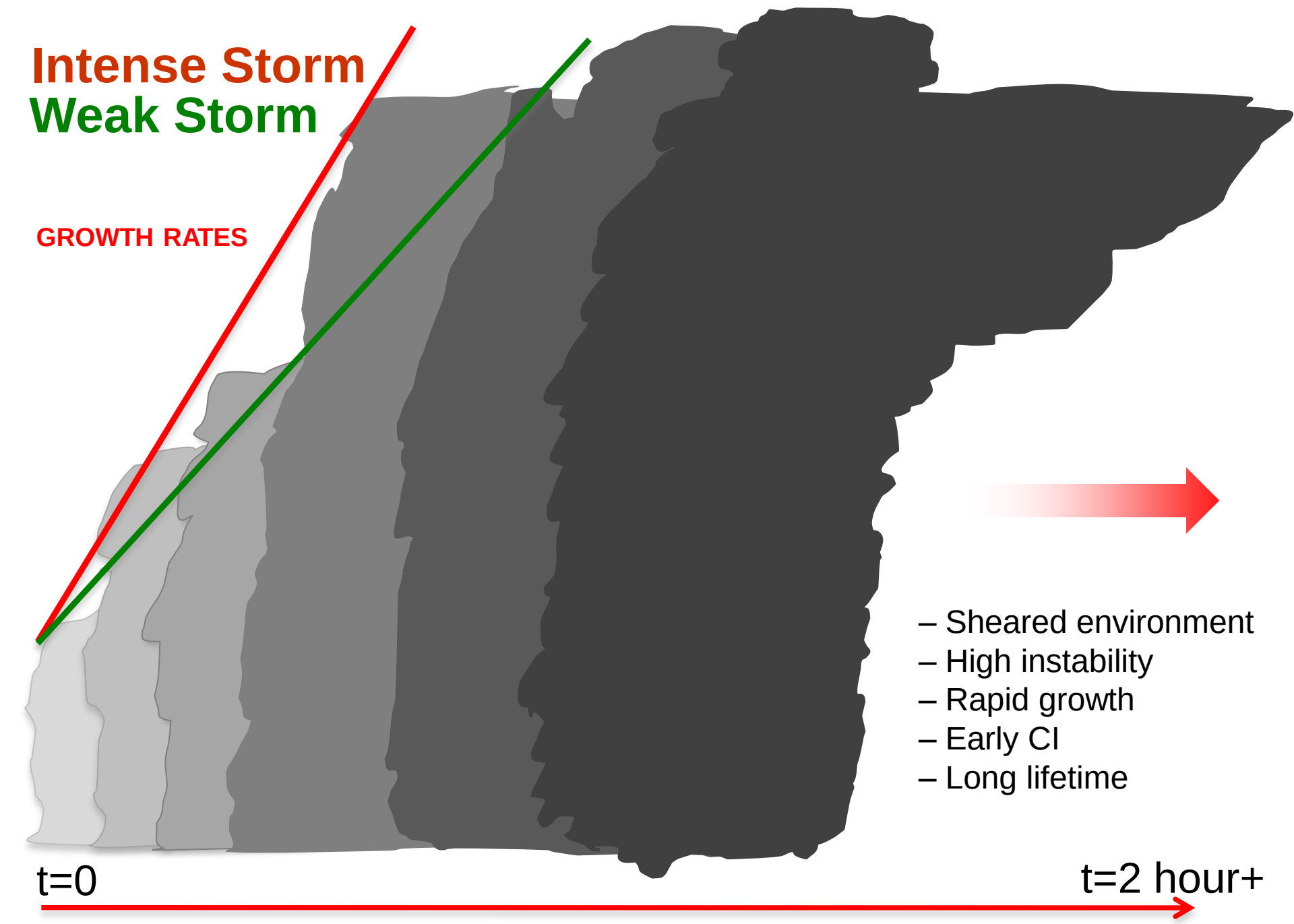

Courtesy Mecikalski

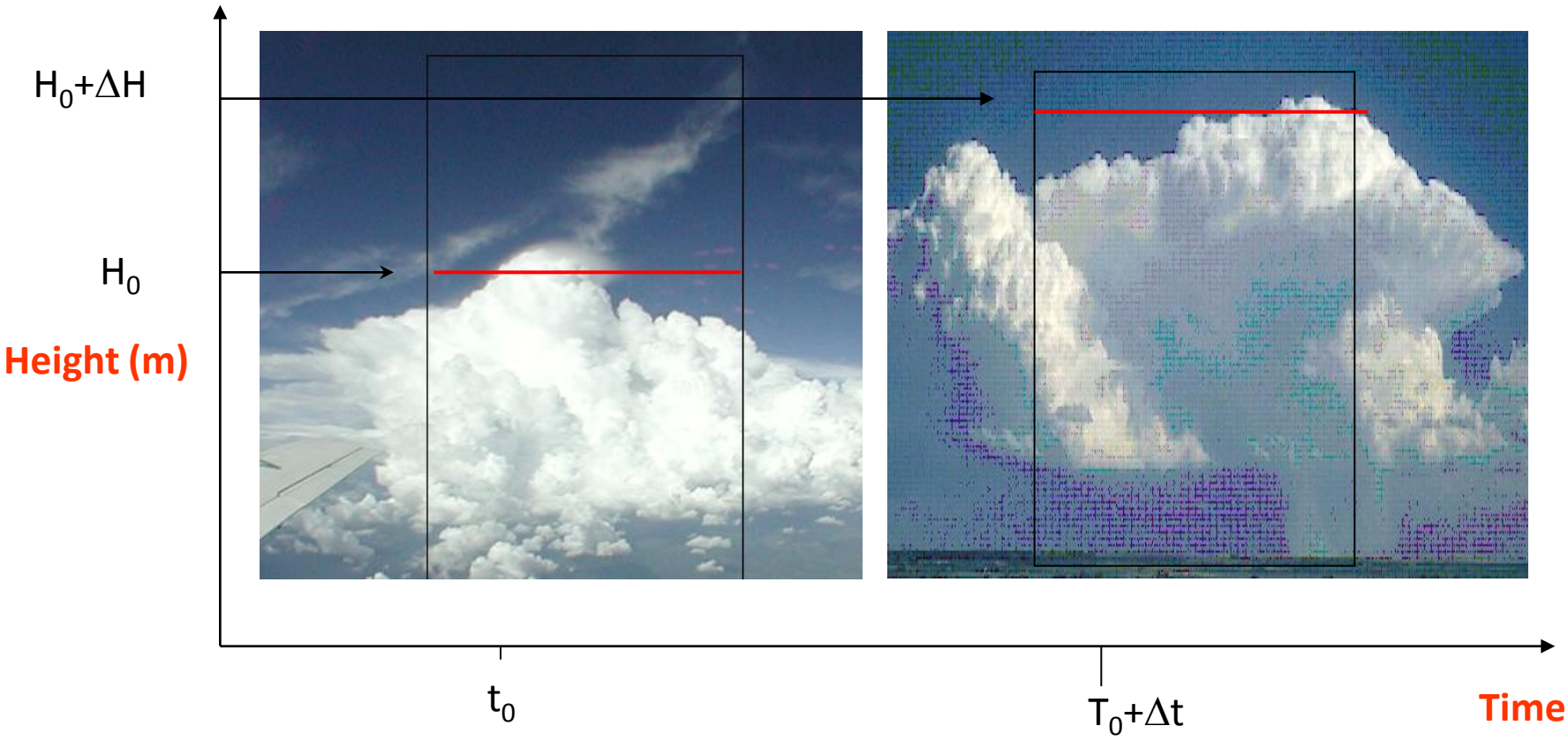

$$W=dH/dt= \{H(t_0)-H(t_0+\Delta t)\}/\Delta t \longrightarrow H(t)=f(20\ dBZ)$$

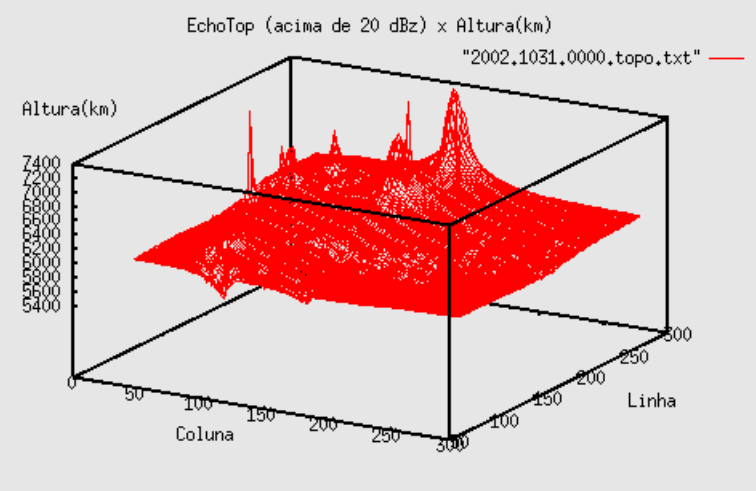
EchoTop (acima de 20 dBz) x Altura(km)
"2002.1031.0000.topo.txt"
Altura(km)
7400
7200
7000
6800
6600
6400
6200
6000
5800
5600
5400
0
50
100
150
200
250
300
Coluna
100
150
200
250
300
Linha

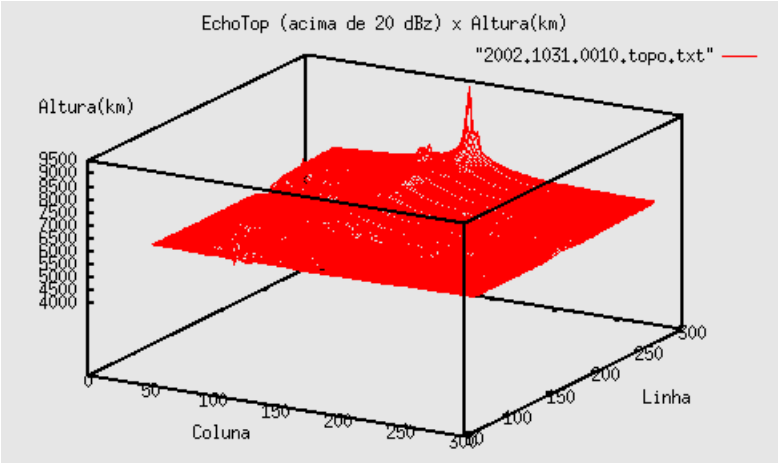
EchoTop (acima de 20 dBz) x Altura(km)
"2002.1031.0010.topo.txt"
Altura(km)
9500
9000
8500
8000
7500
7000
6500
6000
5500
5000
4500
4000
0
50
100
150
200
250
300
Coluna
100
150
200
250
300
Linha

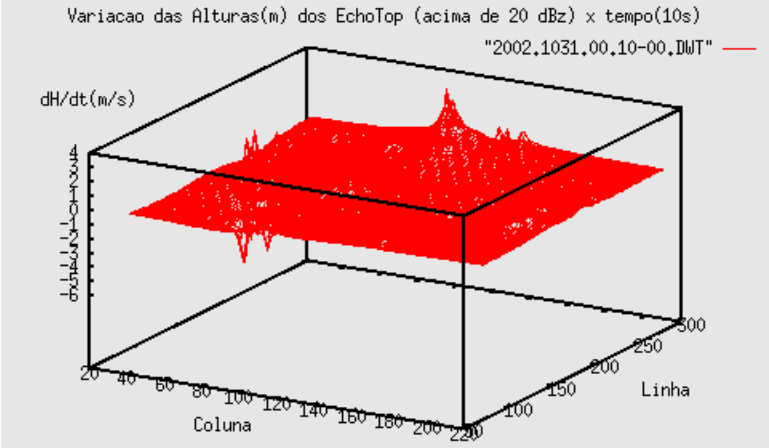
Variacao das Alturas(m) dos EchoTop (acima de 20 dBz) x tempo(10s)
"2002.1031.00.10-00.DWT"
dH/dt(m/s)
20
40
60
80
100
120
140
160
180
200
220
Coluna
100
150
200
250
300
Linha

$$\theta = T.\left(\frac{1000}{P}\right)^{0.286}$$

$$\theta_V = T_V.\left(\frac{1000}{P}\right)^{0.286}$$

$$\theta_e = \left(T.\left(\frac{1000}{P}\right)^{0.286(1-0.28Q)}\right).EXP\left[Q(1+0,81.Q).\left(\frac{3376}{TCOND} - 2.54\right)\right]$$

$$h = c_p T + gz + L_v Q$$

$$CAPE = \frac{1}{g}\int_{FLC}^{NBL}\left(\frac{T_{V_p} - T_{V_e}}{T_{V_e}}\right)dz$$

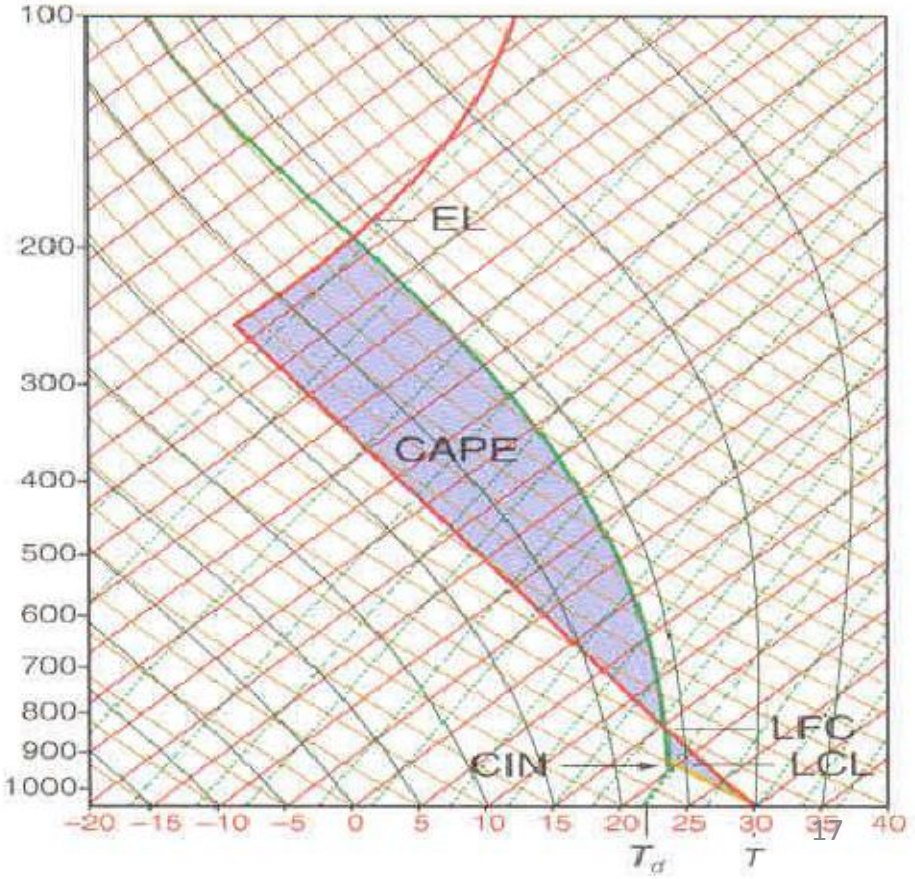

Um valor utilizado para analisar a convecção é o “ Bulk Richardson Number “ que é uma relação entre a energia potencial disponível e a energia cinética disponível.

$$R_i = \frac{CAPE}{\left[\frac{1}{2}\left(\frac{\rho_{700}U_{700} - \rho_{surf}U_{surf}}{(\rho_{700} + \rho_{surf})/2}\right)\right]^2}$$

O cisalhamento do vento é um importante fator na organização do sistema, sistemas convectivos formados em regiões de baixo cisalhamento, terão um tempo de vida curto, pois grande parte da água condensada nos updrafts precipitarão na mesma região, inibindo as correntes ascendentes, ao contrário, sistemas formados em ambientes com alto cisalhamento, grande parte da água condensada será advectada para o anvil. Assim sendo, o cisalhamento do vento poderia ser utilizado para regular a quantidade de água evaporada para o anvil, a seguir apresentamos uma sugestão para esta parametrização:

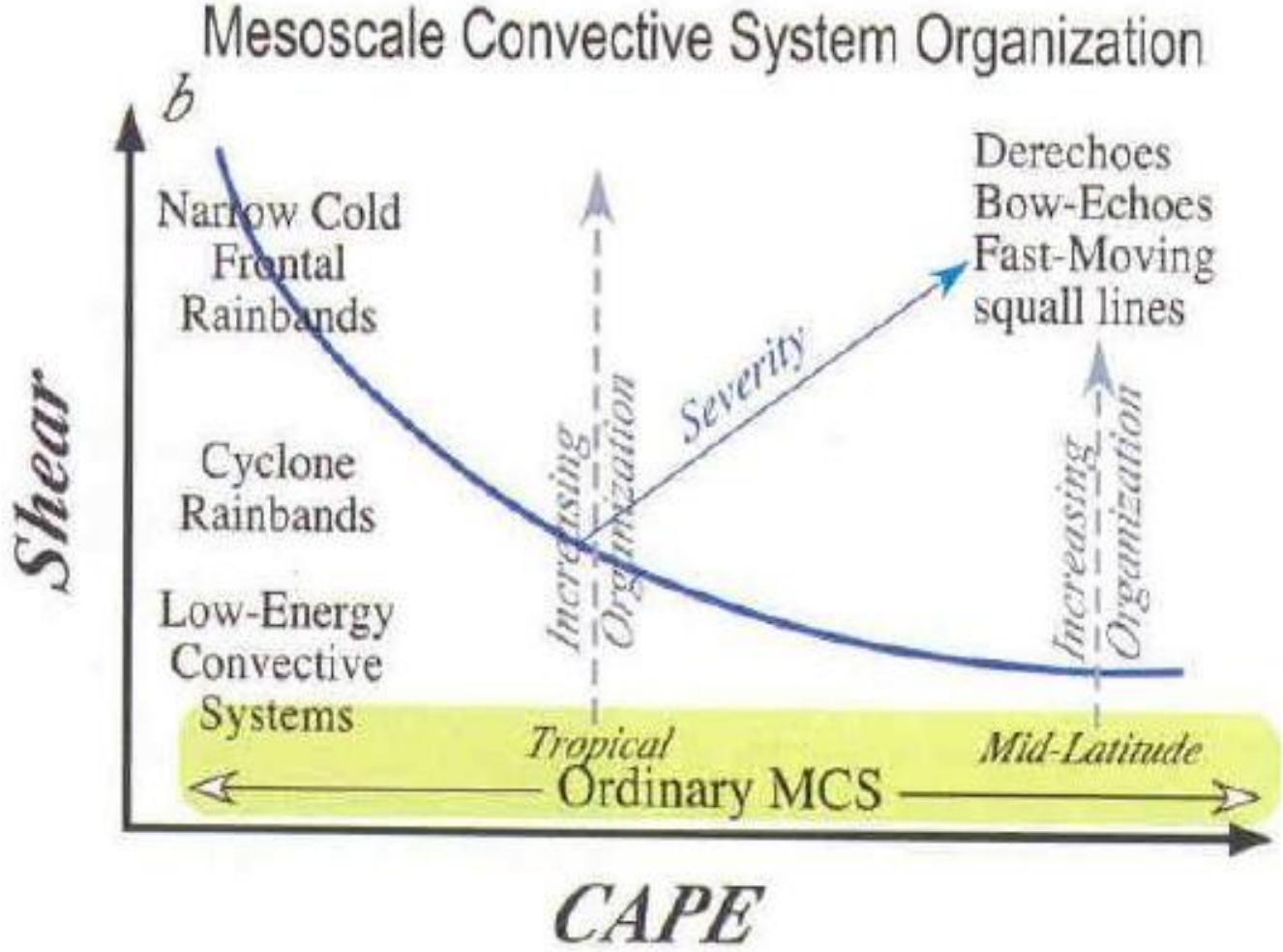
Mesoscale Convective System Organization
b
Shear
Narrow Cold Frontal Rainbands
Cyclone Rainbands
Low-Energy Convective Systems
Increasing Organization
Severity
Derechoes Bow-Echoes Fast-Moving squall lines
Increasing Organization
Tropical
Mid-Latitude
Ordinary MCS
CAPE

Rain Cells and the Richardson Space

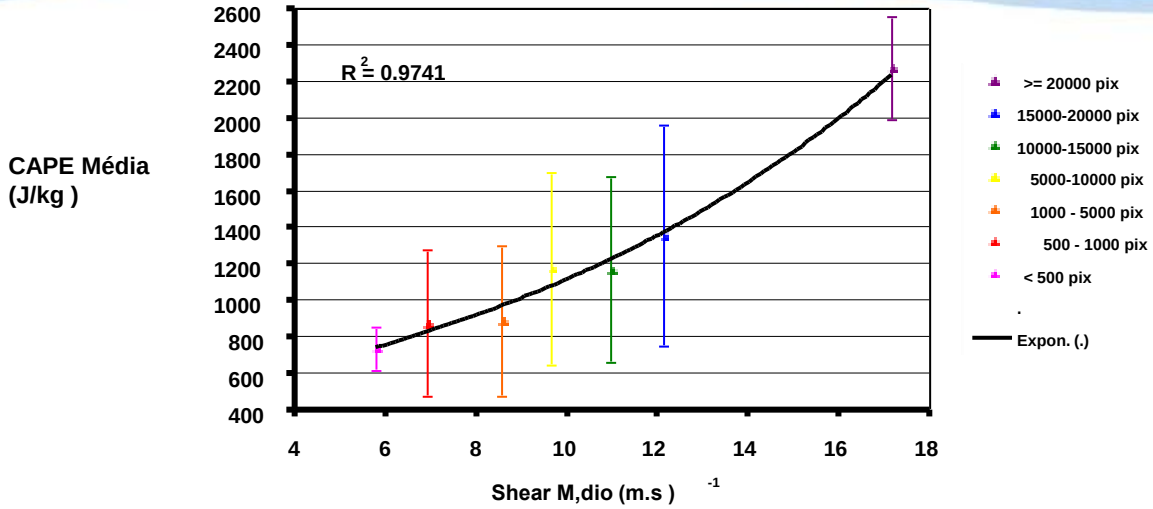

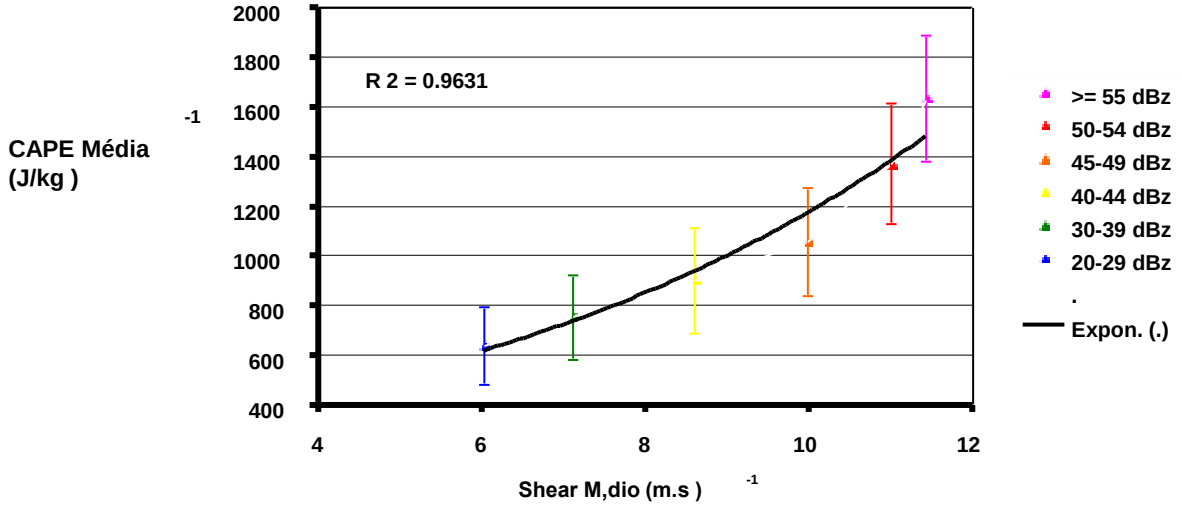

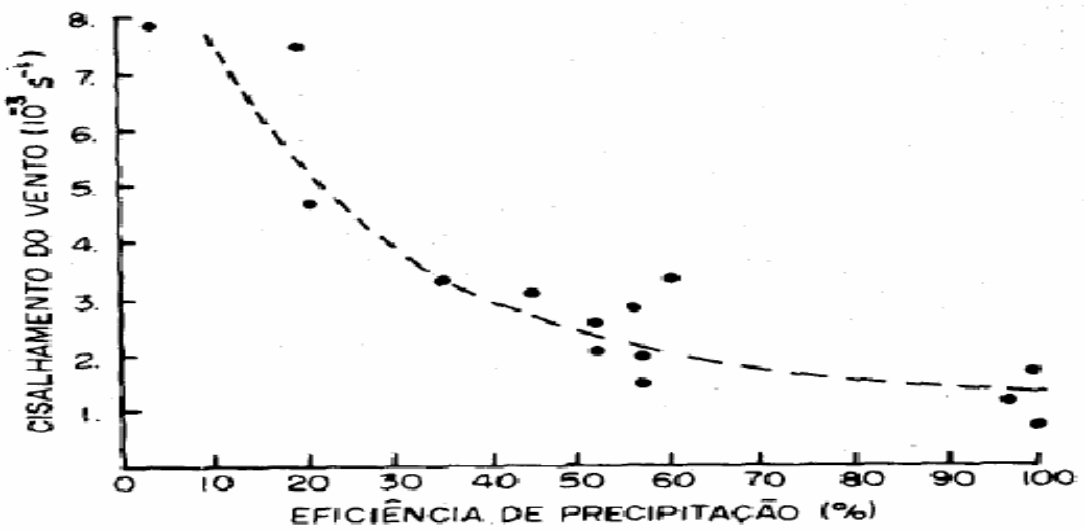

Figura 2 — Diagrama de dispersão do cisalhamento do vento versus eficiência de precipitação para 14 tempestades que ocorreram nas Altas Planícies da América do Norte. A linha tracejada foi manualmente ajustada aos dados. (Marwitz, 1972).

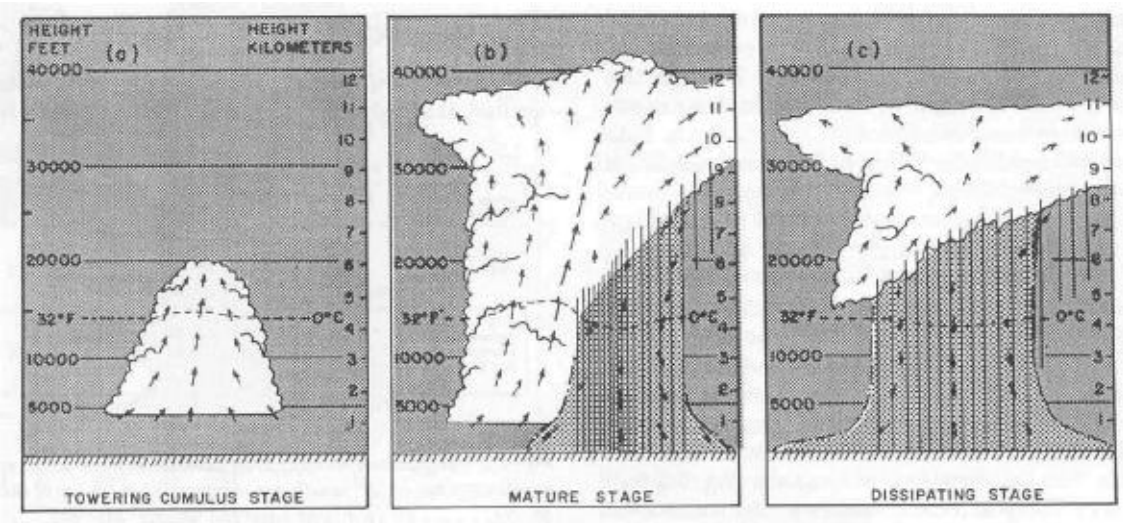

Niamey - 2006 - AMMA Experiment

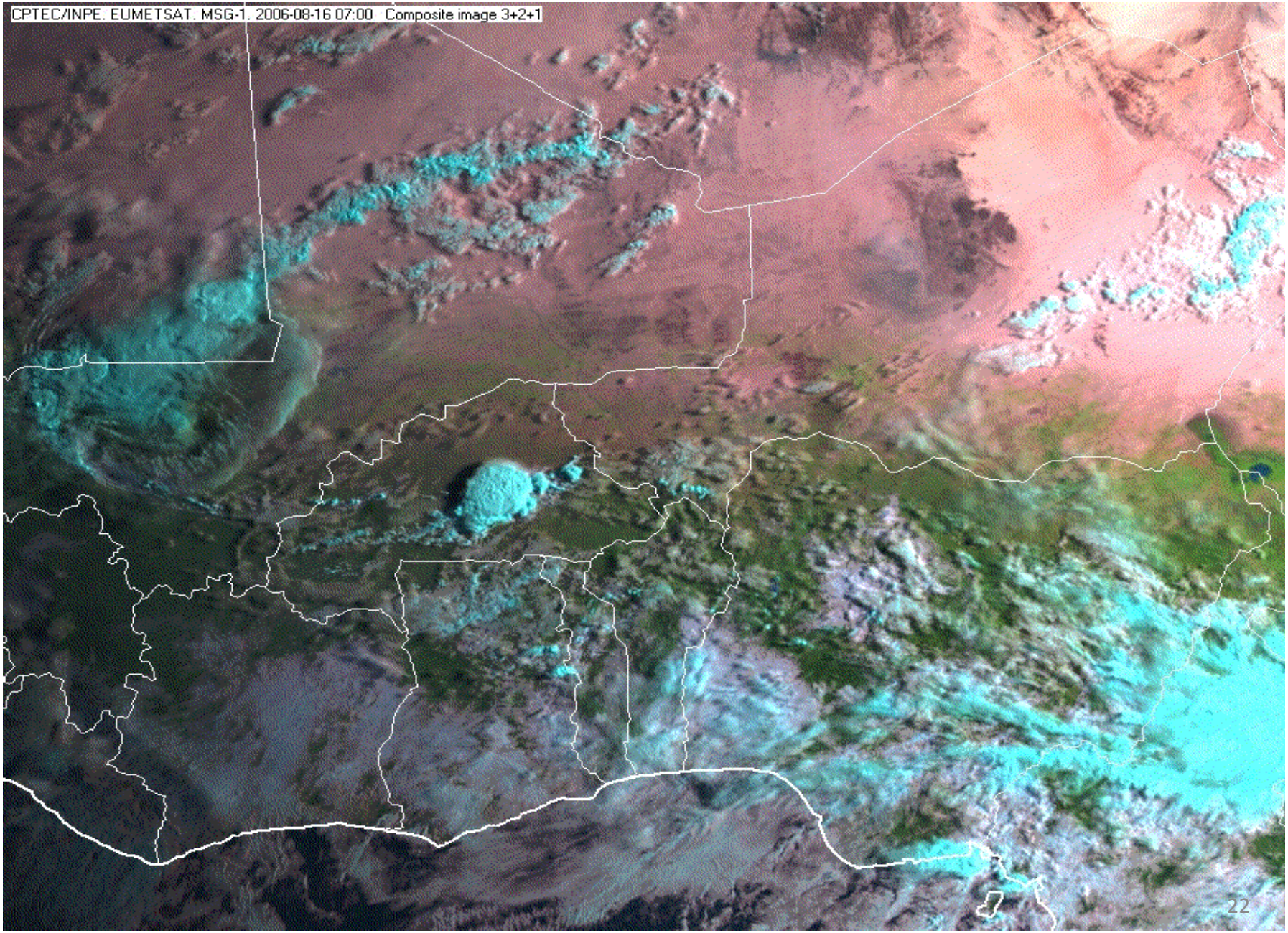

Interação Brisa e Frente de Rajada

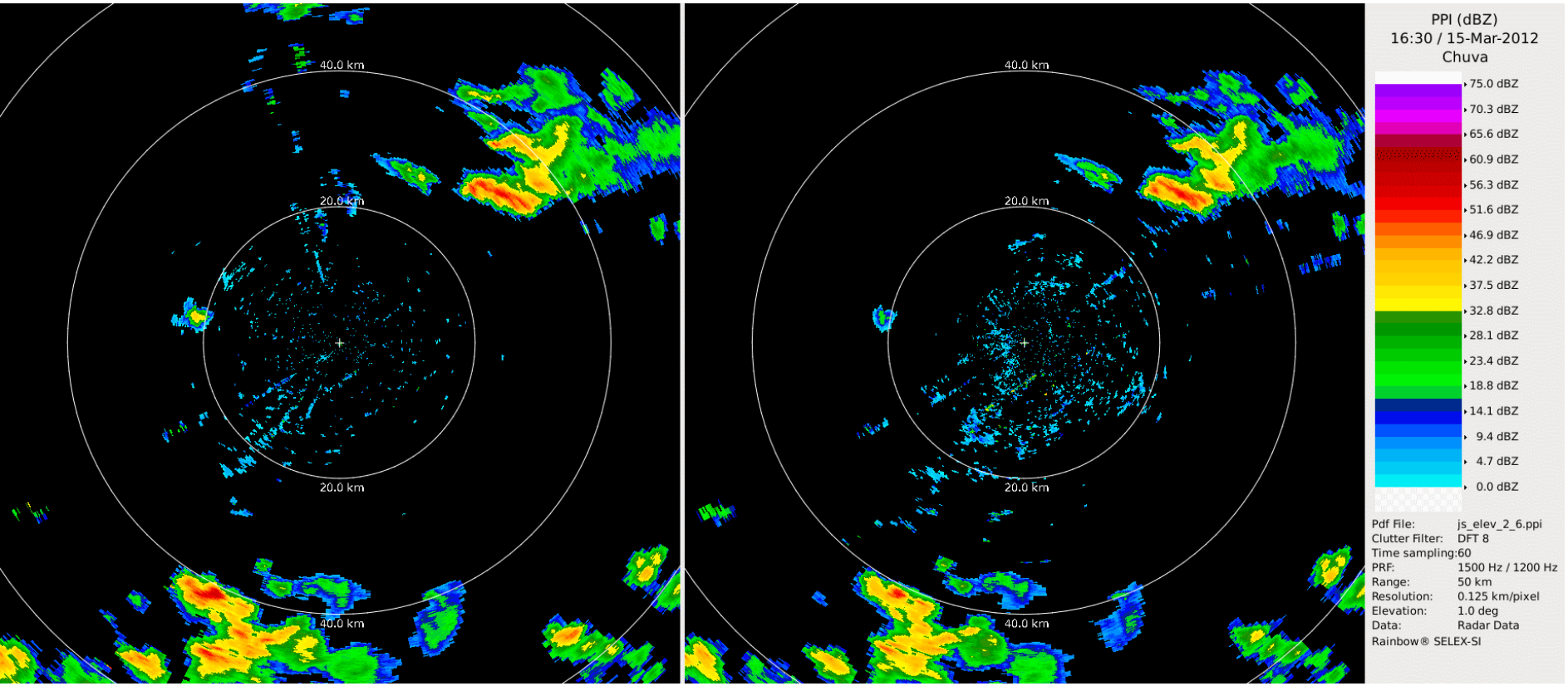

Sea Breeze

Sea Breeze

First Convective Cells formed in Matiqueira Mountains

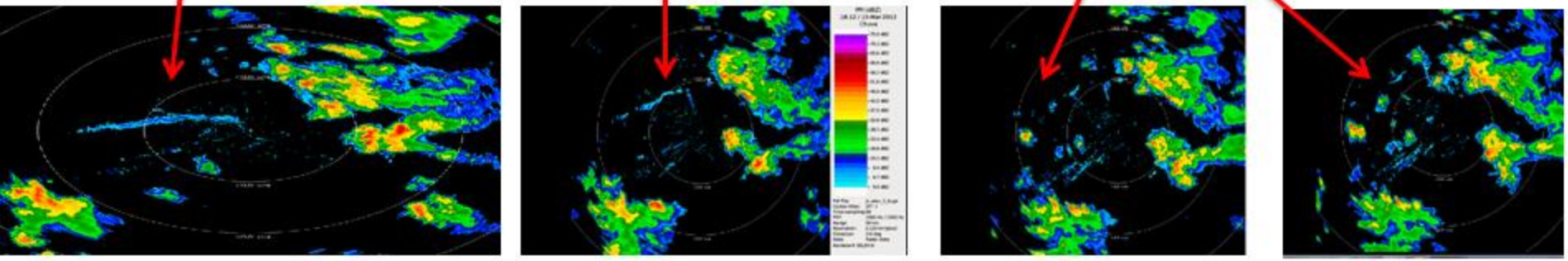

Gust Front

First Convective Cells formed trought the interaction between Sea Breeze and Gust Front

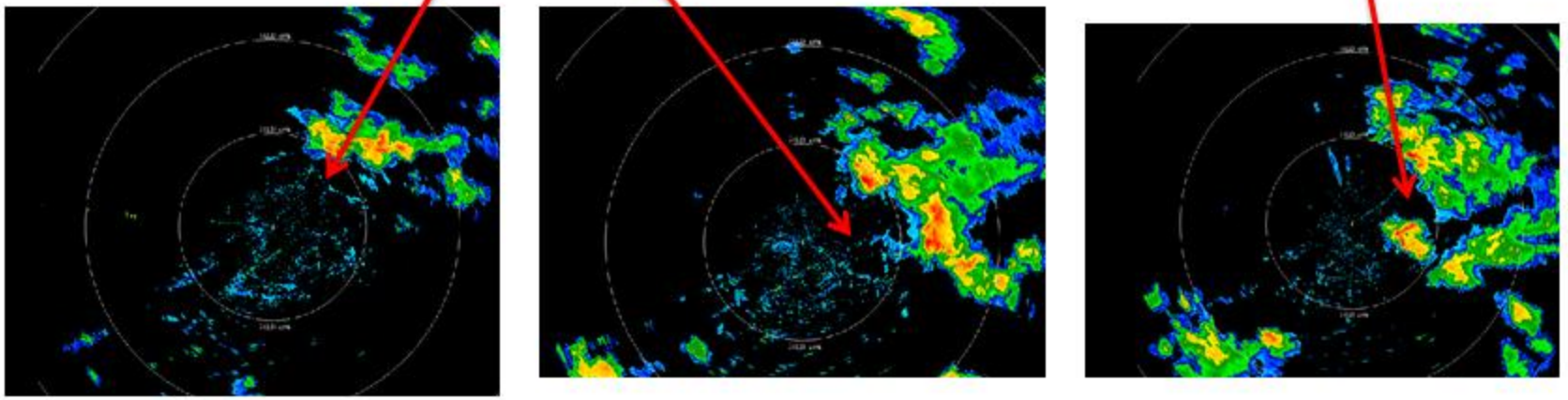

APPROACHING MORNING SQUALL LINE ON AGUST 6, 2006

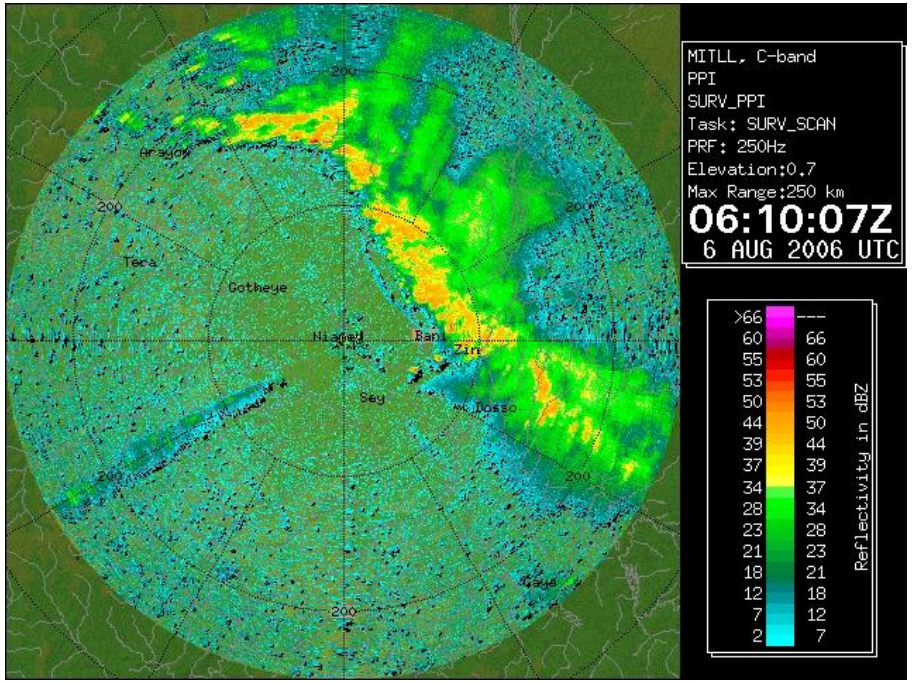

Courtesy E. Willians

GUST FRONT

Gust Front Sweeping out Noctural Insect Population on July 4, 2006

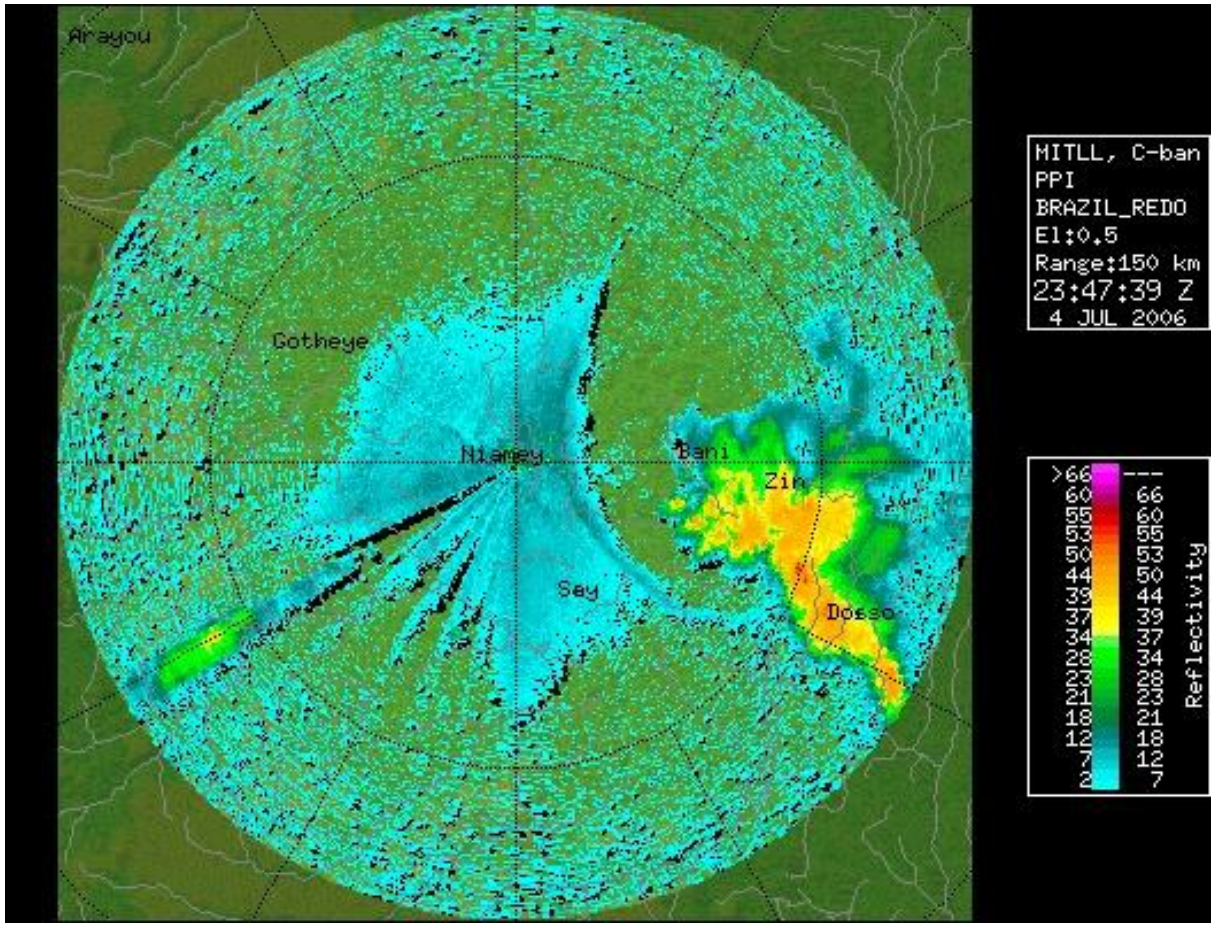

Courtesy E. Willians

GUST FRONTS AT CONVECTIVE SCALE AND MESOSCALE

Thunderstorm microbust on July 10, 2006

Gust Front leading squall line on September 12, 2006

Courtesy E. Willians

METEOSAT DEPICTION OF LARGE SCALE IMPACT OF THUNDERSTORM DOWNDRAFT

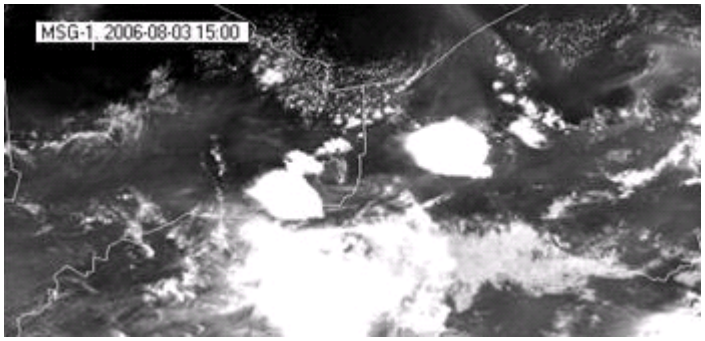

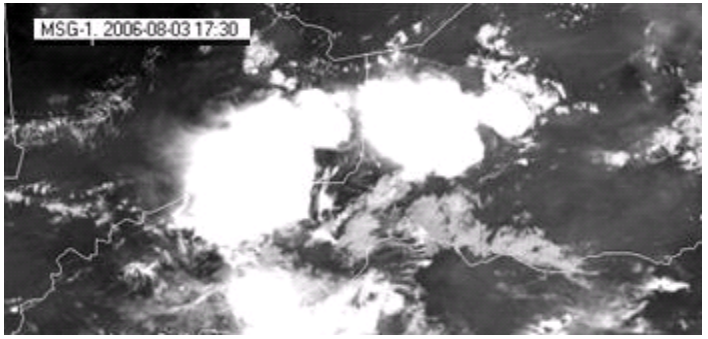

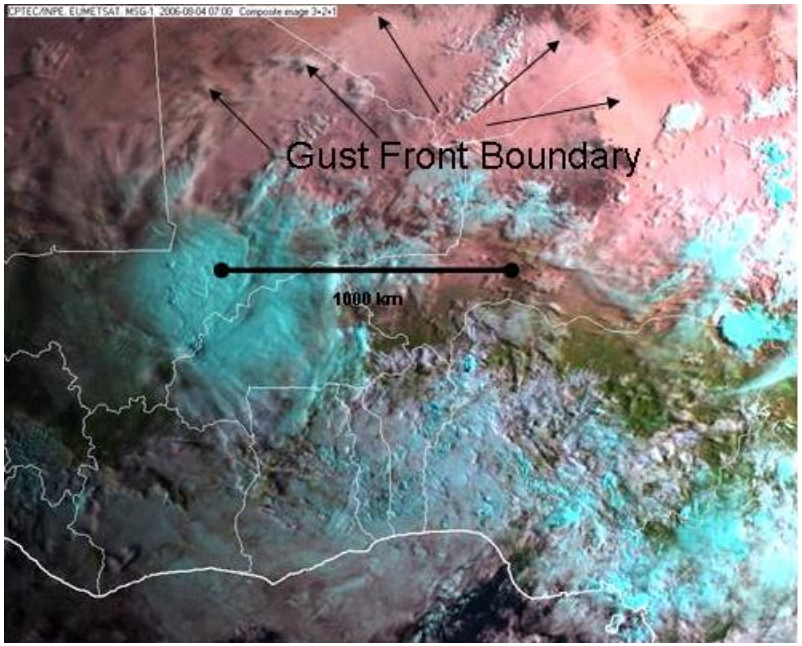

IS SOIL COMPOSITION A DISCRIMINANT FOR ORIGIN OF DUST ?

SAHARA

DESERT

White/Yellow Sand

SAHEL

Red Soil

Courtesy E. Willians

Transport of Africa Aerosol to the Amazonia

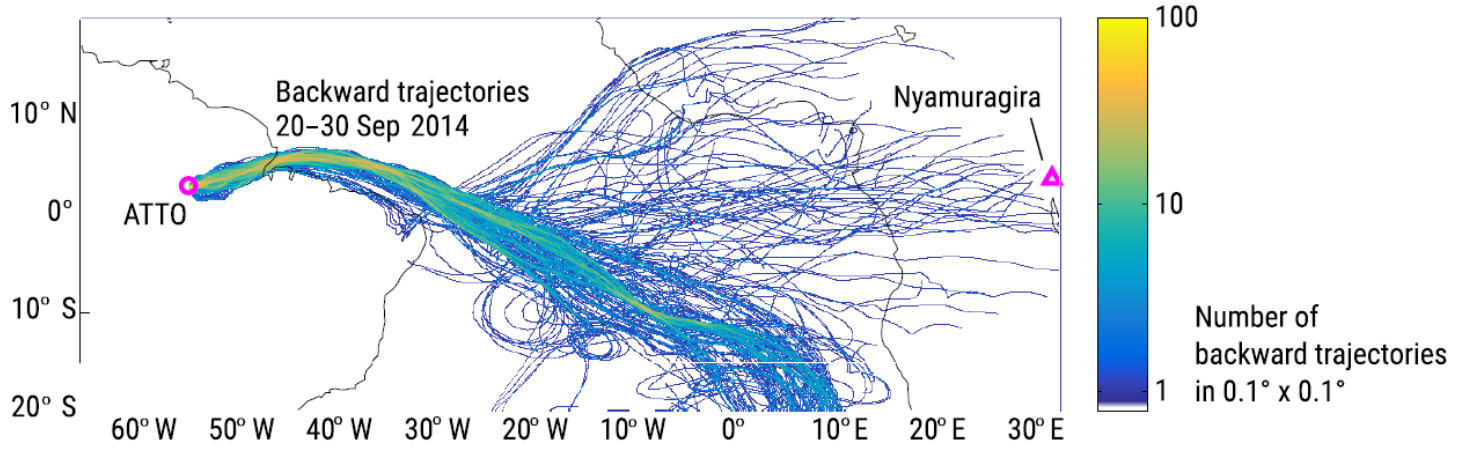

Figure 5. Density of 15-day backward trajectories started from ATTO at an altitude of 300 m a.m.s.l. every hour starting at 00:00 UTC on 20 September 2014 to 23:00 UTC on 30 September 2014.

Saturno, J., Ditas, F., Penning de Vries, M., Holanda, B. A., Pöhlker, M. L., Carbone, S., Walter, D., Bobrowski, N., Brito, J., Chi, X., Gutmann, A., Hrabe de Angelis, I., Machado, L. A. T., Moran-Zuloaga, D., Rüdiger, J., Schneider, J., Schulz, C., Wang, Q., Wendisch, M., Artaxo, P., Wagner, T., Pöschl, U., Andreae, M. O., and Pöhlker, C.: African volcanic emissions influencing atmospheric aerosols over the Amazon rain forest, Atmos. Chem. Phys., 18, 10391-10405, https://doi.org/10.5194/acp-18-10391-2018, 2018.

Transport of Africa Aerosol to Amazonia in the 3-5 km layer.

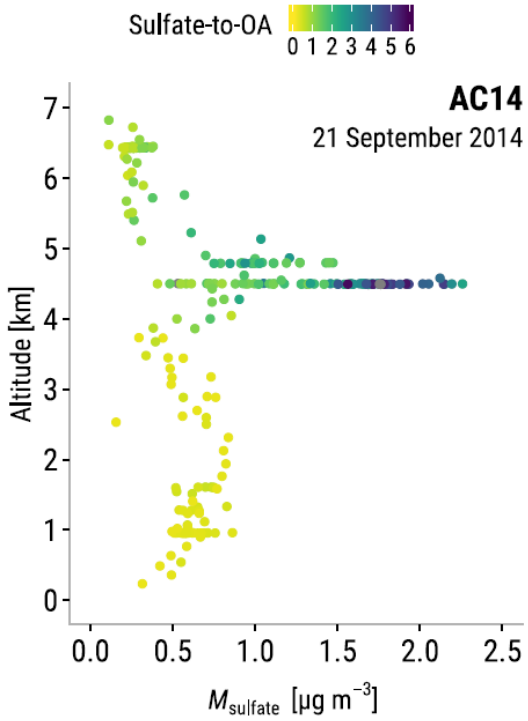

Figure 6. Sulfate layer observations over the Amazon rain forest. The figure shows the $M_{sulfate}$ vertical profile observed during flight AC14 (21 September 2014). Color-coded sulfate-to-OA values are truncated at a maximum of 6.

MAM – LLJ

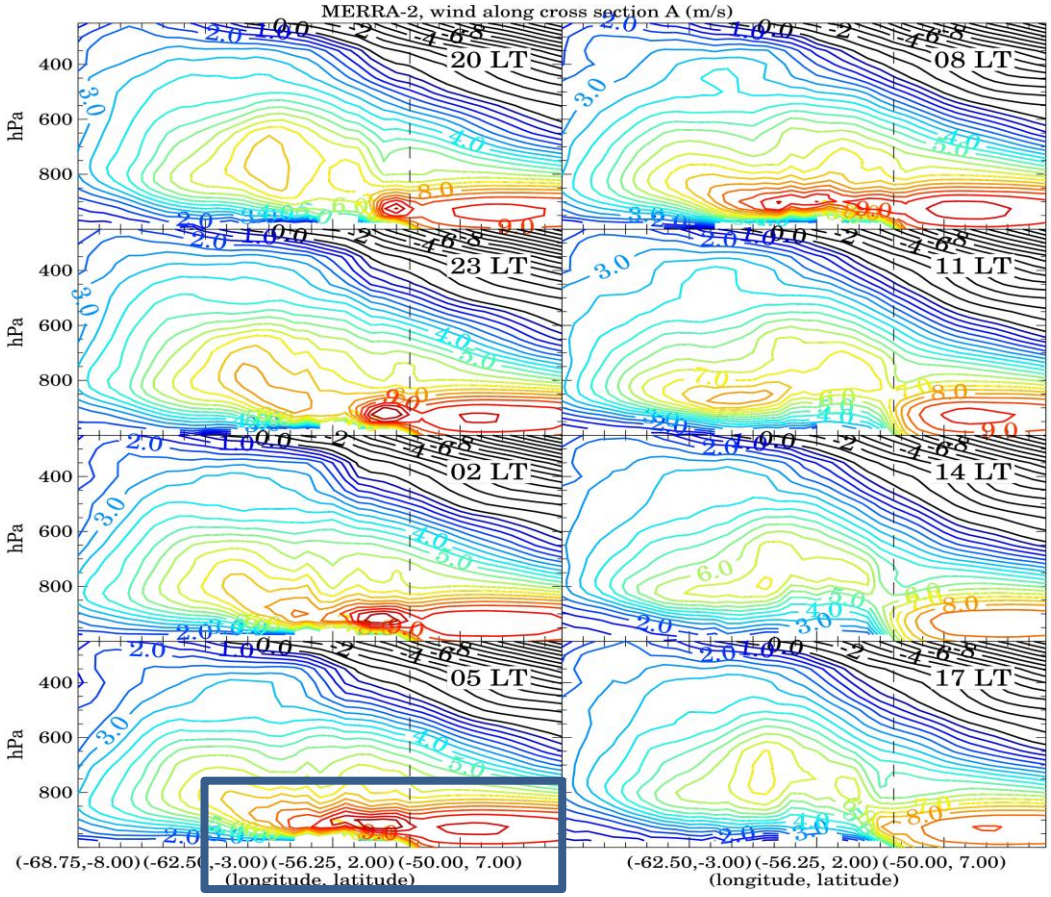
MERRA-2, wind along cross section A (m/s)
20 LT
08 LT
23 LT
11 LT
02 LT
14 LT
05 LT
17 LT
hPa
400
600
800
(-68.75,-8.00) (-62.50,-3.00) (-56.25, 2.00) (-50.00, 7.00)
(longitude, latitude)
(-62.50,-3.00) (-56.25, 2.00) (-50.00, 7.00)
(longitude, latitude)

Upper Tropospheric Transport

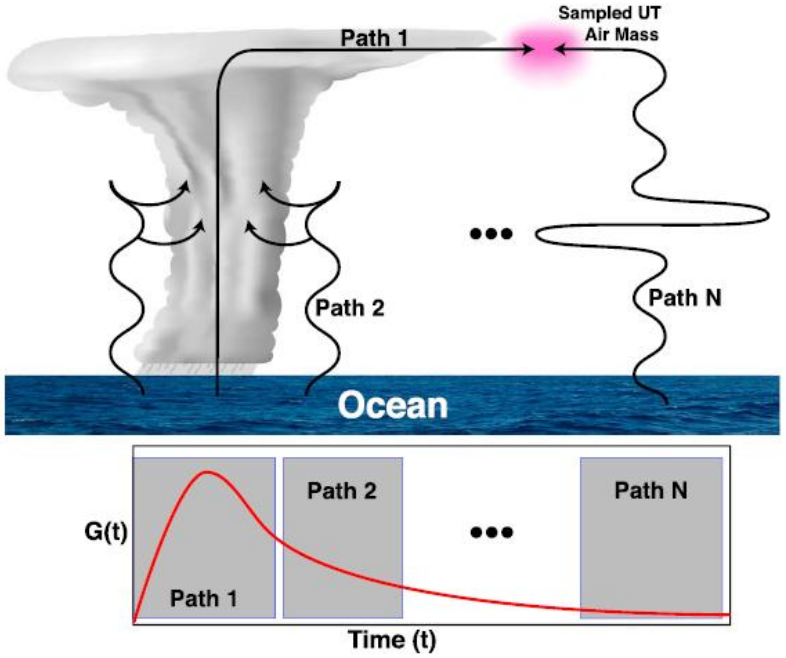

Figure 1. Schematic of transport paths in the convectively dominant tropical western Pacific. A transit time spectrum, *G(t)*, is defined to describe the relative contributions of these different paths. UT = upper troposphere.

Table 1
VOCs and Tropospheric Lifetimes Used to Generate the Transit Time Spectrum

ID	Instrument	VOC	Lifetime [days]	Source of estimate
1	TOGA	Acetaldehyde, CH_3CHO	0.25	Calculated
2	AWAS	DMS, $(CH_3)_2S$	0.96	Calculated
3	AWAS	n-Pentane, C_5H_{12}	1.2	Calculated
4	TOGA, AWAS	n-Butane, C_4H_{10}	1.9	Calculated
5	TOGA, AWAS	Isobutane, $CH(CH_3)_3$	2.1	Calculated
6	AWAS	n-Butyl Nitrate, $C_4H_9ONO_2$	2.2	Calculated
7	AWAS	2-Butyl Nitrate, $C_2H_5CH(CH_3)ONO_2$	3.8	Calculated
8	TOGA, AWAS	Benzene, C_6H_6	3.8	Calculated
9	TOGA, AWAS	Propane, C_3H_8	4.2	Calculated
10	TOGA	Methanol, CH_3OH	5.2	Calculated
11	AWAS	Ethyne, C_2H_2	6.0	Calculated
12	AWAS	Isopropyl Nitrate, $CH(CH_3)_2ONO_2$	6.4	Calculated
13	AWAS	Chlorobenzene, C_6H_5Cl	9.2	Calculated
14	AWAS	Ethyl Nitrate, $C_2H_5ONO_2$	11	Calculated

The Hole

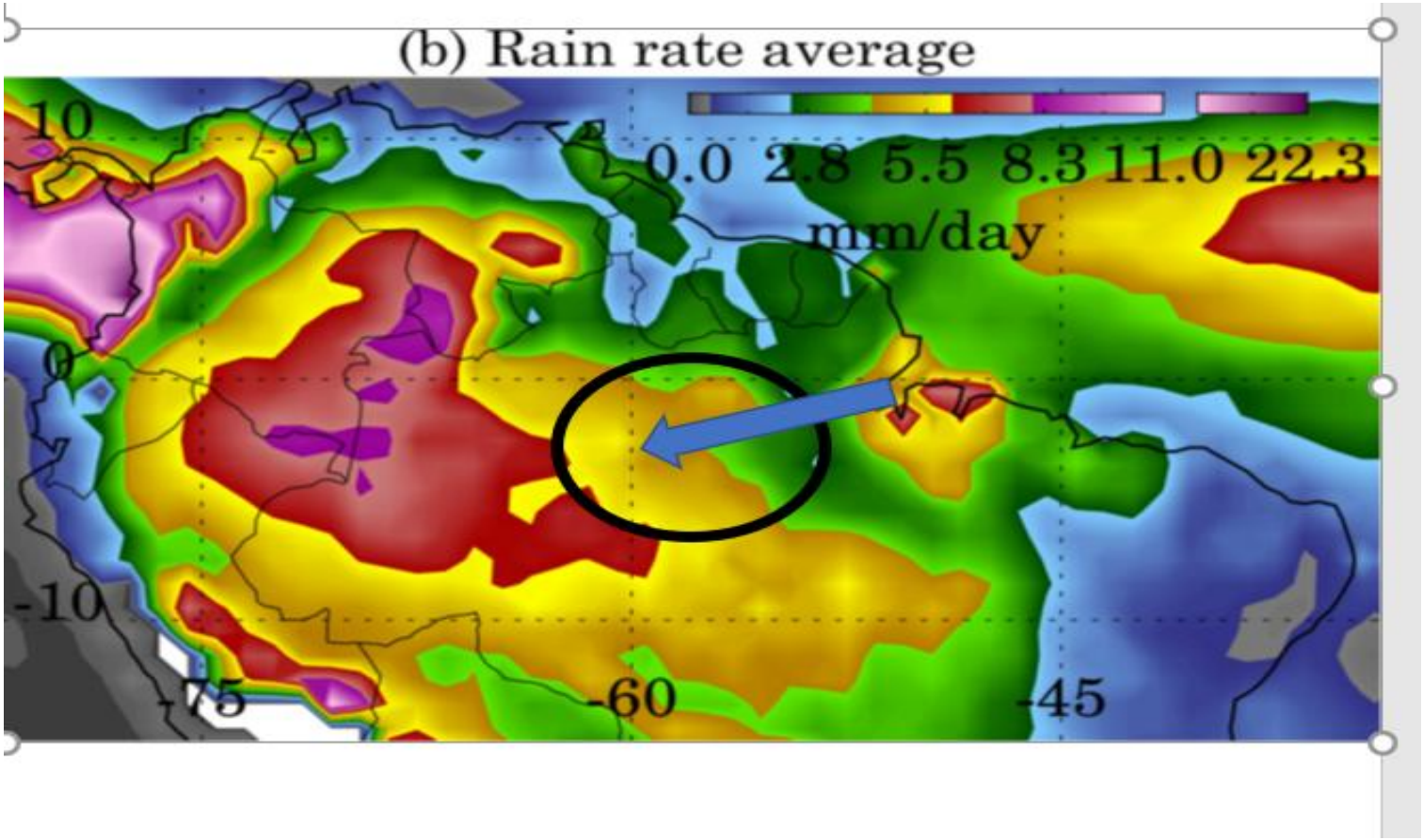

Chemistry Profiles

OutFlow Convection (Wang)

4-5 km – most of biomass burning from Africa (bruna Holanda)
4-5 km - transport of volcanogenic aerosols (Saturno)

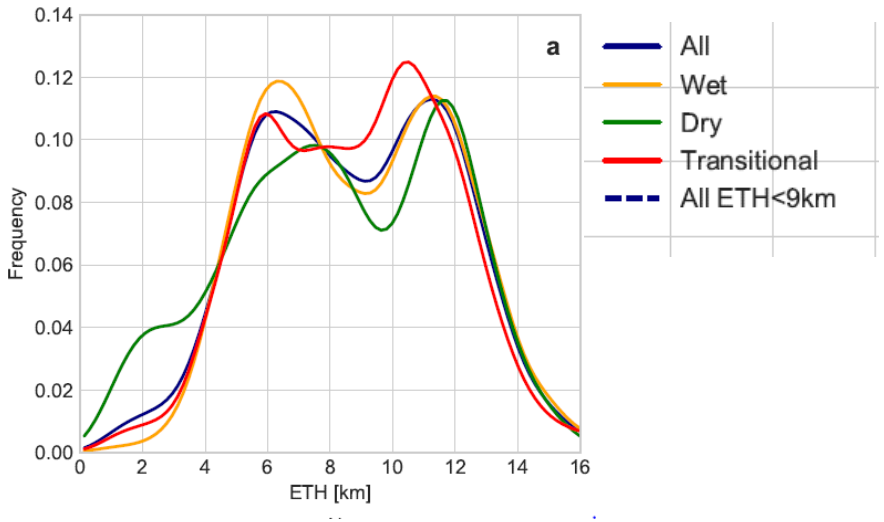

Convective Clouds and Aerosol feedbacks

Surface ozone modulation by convective processes

Downward transport of ozone rich air and implications for atmospheric chemistry in the Amazon rainforest by Tobias Gerkena,, Dandan Weia, Randy J. Chasea, Jose D. Fuentesa, Courtney Schumacherf, Luiz A. T. Machado, Marcelo Chameckia, Livia S. Freirea, Angela B.ardinec, Antonio O. Manzic, Rosa M. Nascimento dos Santose, Celso von Randowd, Paul C. Stoyg, Julio Totah, Amy M. Trowbridge **Atmospheric Environment, 2016**

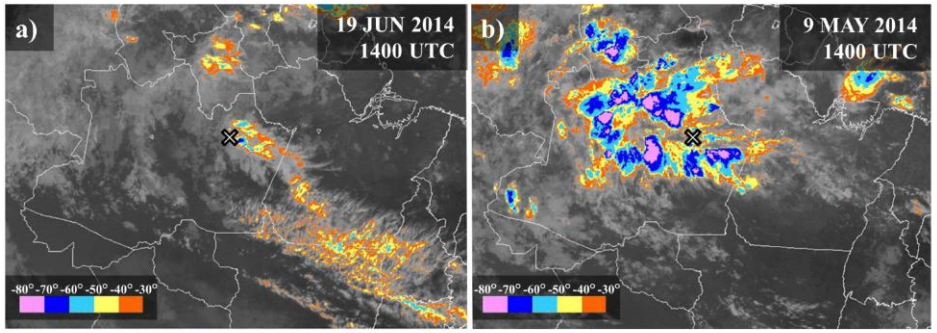

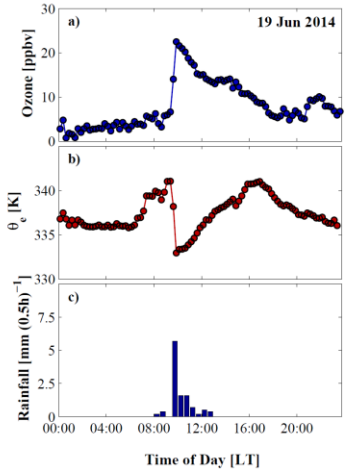

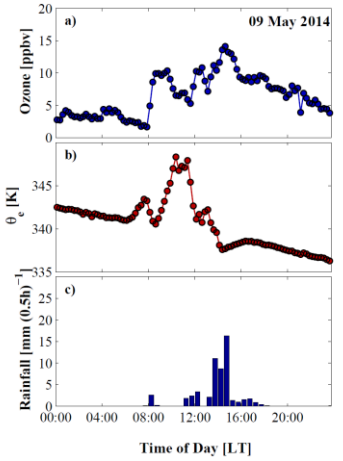

Convective Clouds and Aerosol feedbacks

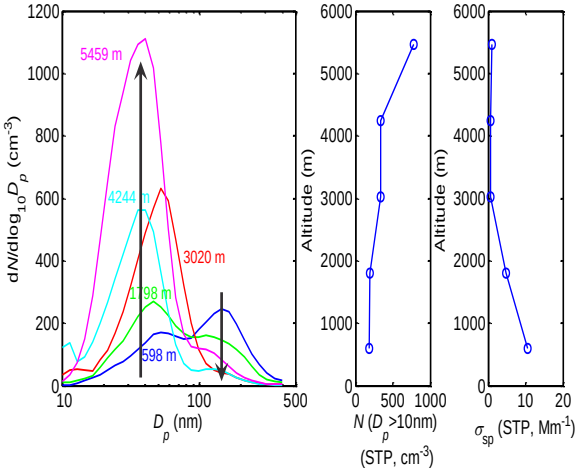

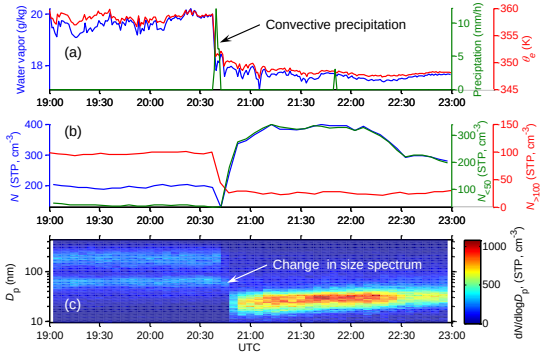

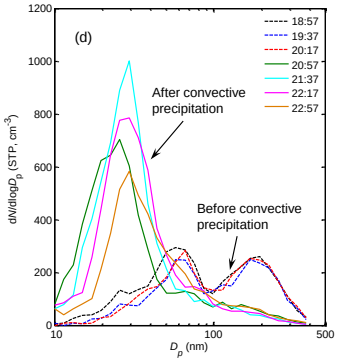

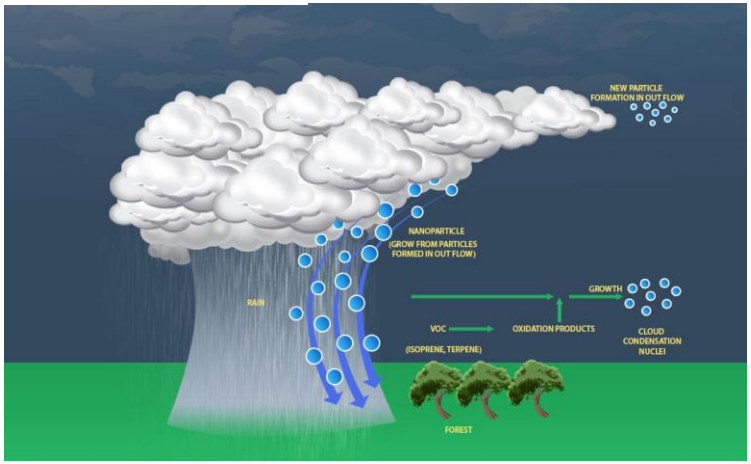

Deep convections sustain aerosol concentration in Amazon atmosphere
by *Jian Wang, Radovan Krejci, Scott Giangrande, Chongai Kuang, Hanna E. Manninen, Henrique M. J. Barbosa, Joel Brito, Jennifer Comstock, Mira Krüger, Jost Lavric, Karla Longo, Antonio O. Manzi, Fan Mei, Christopher Pöhlker, Beat Schmid, Rodrigo A. F. Souza, Steven Springston, Jason Tomlinson, David Walter, Daniela Wimmer, Jim Smith, Markku Kulmala, Luiz A. T. Machado, Paulo Artaxo, Meinrat Andreae, Scot Martin, Tuukka Petaja* – ***Nature 2016***

Convective Clouds and Aerosol feedbacks

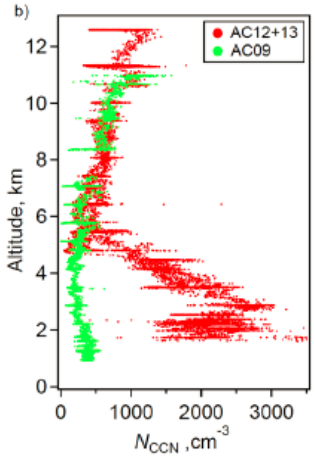

The air in the immediate outflow of deep convective clouds was depleted in aerosol particles, whereas strongly enhanced number concentrations of small particles (<90 nm diameter)

Figure 7: Vertical profiles of CN concentrations, N_{CN}; a) overall statistics from all flights, b) examples from individual profiles on flight AC07 (segment G) and AC09 (segments A1 and A2).

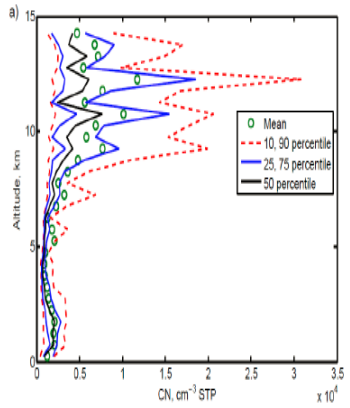

Aerosol characteristics and particle production in the upper troposphere over the Amazon Basin

Meinrat O. Andreae, Armin Afchine, Rachel Albrecht, Bruna Amorim Holanda, Paulo Artaxo, Henrique M. J. Barbosa, Stephan Borrmann, Micael A. Cecchini, Anja Costa, Maximilian Dollner, Daniel Fütterer, Emma Järvinen, Tina Jurkat, Thomas Klimach, Tobias Konemann, Christoph Knote, Martina Krämer, Trismono Krisna, Luiz A. T. Machado, Stephan Mertes, Andreas Minikin, Christopher Pöhlker, Mira L. Pöhlker, Ulrich Pöschl, Daniel Rosenfel, Daniel Sauer, Hans Schlager, Martin Schnaiter, Johannes Schneider,Christiane Schulz, Antonio Spanu, Vicinius B. Sperling, Christine Voigt, Adrian Walser, Jian Wang, Bernadett Weinzier, Manfred Wendisch, and Helmut Ziereis.

Atmos. Chem. Phys. Discuss., https://doi.org/10.5194/acp-2017-694

Figure 24: Conceptual model of the aerosol life cycle over the Amazon Basin

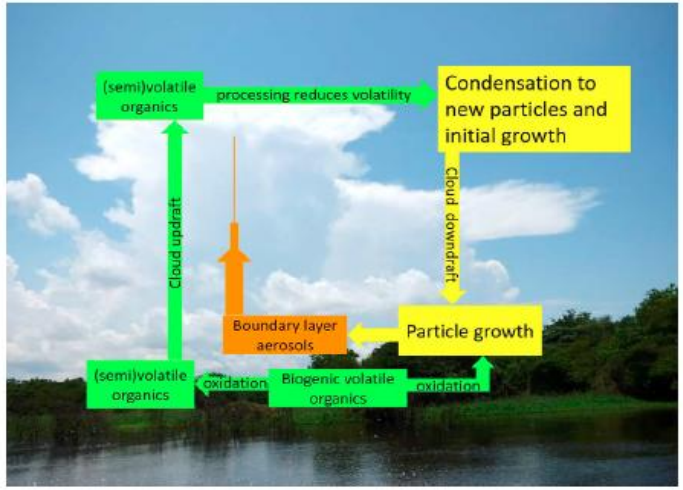

Conceptual model, where production of new aerosol particles takes place in the UT from **biogenic volatile organic material brought up by deep convection**, which is converted to condensable species in the UT. Subsequently, downward mixing and transport of upper tropospheric aerosol can be a source of particles to the PBL, where they increase in size by the condensation of biogenic volatile organic carbon (BVOC) oxidation products

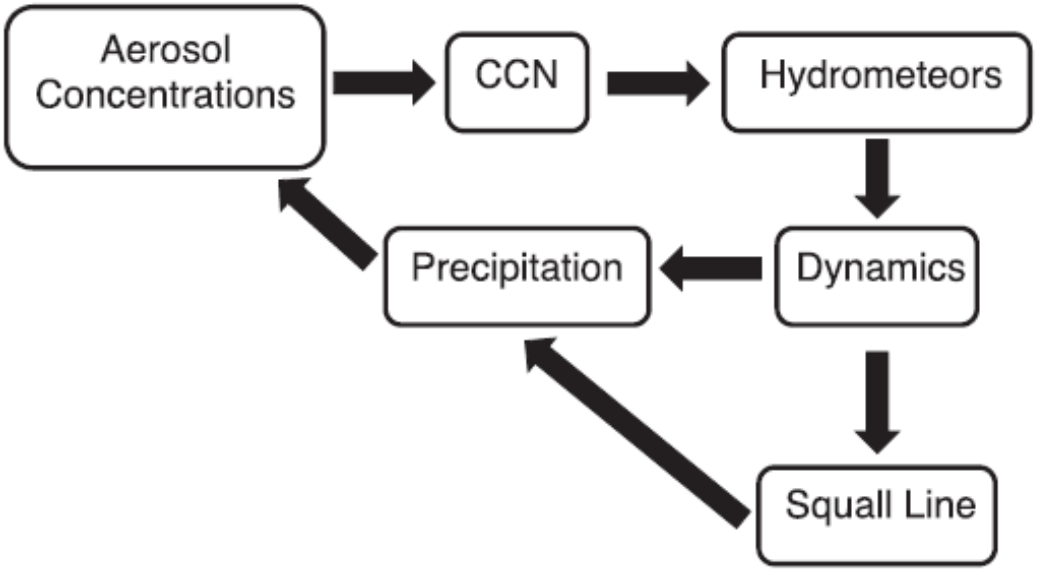

FIG. 11. Schematic that describes the processes affected by changing urban emissions. Aerosol concentrations are directly affected by scaling urban emissions, which lead to changes in the number of CCN available and the growth and formation of hydrometeors. The growth and formation of hydrometeors affect the dynamics of the squall-line changes. The differences in the squall-line propagation ultimately lead to a different precipitation spatial pattern and altered aerosol concentrations.

Kawecki, S., G.M. Henebry, and A.L. Steiner, 2016: Effects of Urban Plume Aerosols on a Mesoscale Convective System. *J. Atmos. Sci.,* **73**, 4641–4660,https://doi.org/10.1175/JAS-D-16-0084.1

During phase I,

doubling urban emissions shifts the precipitation accumulation, with enhancement downwind of the storm propagation and suppression upwind.

During phase II,

a squall line develops in the baseline and doubled emissions scenarios but not when emissions are halved. These changes in MCS propagation and strength are a function of cold pool strength, which is determined by microphysical processes and directly influenced by aerosol load.

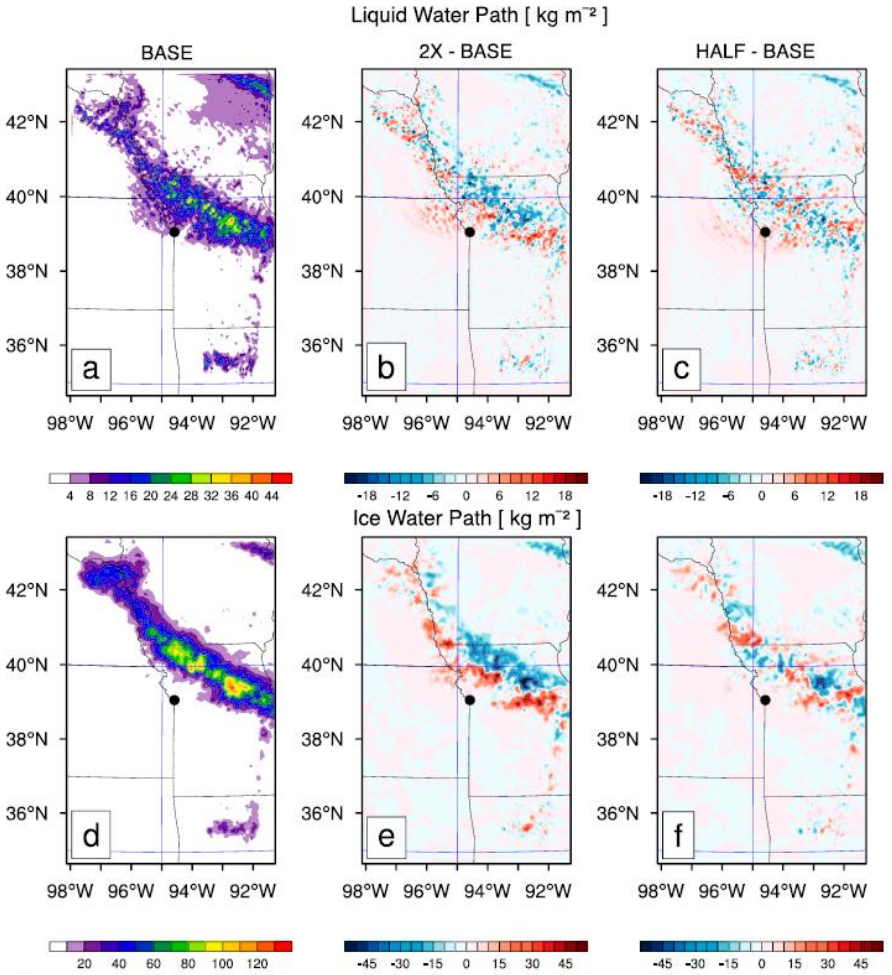

FIG. 6. Phase I (1800 UTC 26 May–0600 UTC 27 May) ensemble-average temporally integrated (a)–(c) liquid and (d)–(f) ice water paths. (a) BASE case LWP. (b) 2X − BASE LWP. (c) HALF − BASE LWP. (d) BASE case IWP. (e) 2X − BASE IWP. (f) HALF − BASE IWP. For difference plots, red shades indicate an increase in LWP and IWP due to the emissions change; blue shades indicate a decrease in LWP and IWP due to the emissions change. The black dot indicates the location of Kansas City, MO.

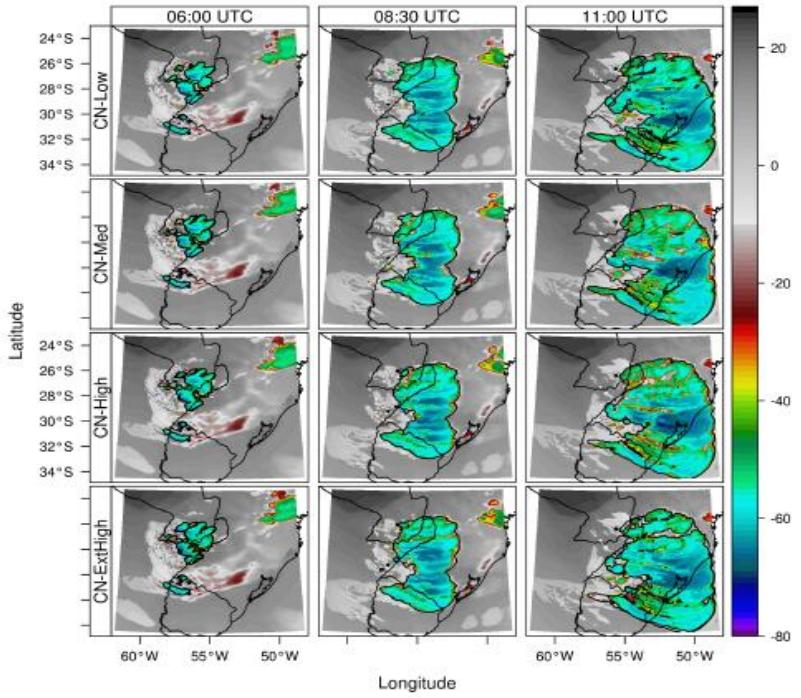

Figure 3.5: Synthetic infrared satellite images for the CN-Low, CN-Med, CN-High and CN-ExtHigh experiments at 06:00 (left panels), 08:30 (middle panels) and 11:00 UTC (right panels). Colors indicate brightness temperature at channel 10.7 μm. The black contour line refers to the brightness temperature equal to -32 °C, which delimits the MCS area (Maddox, 1980).

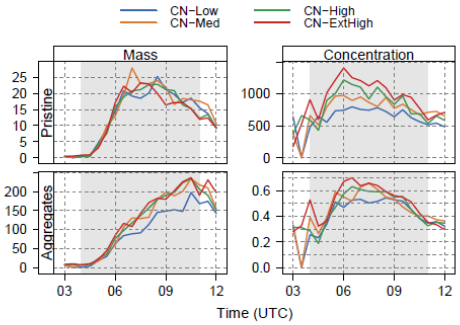

Figure 3.11: As in Figure 3.9, but for pristine and aggregate categories.

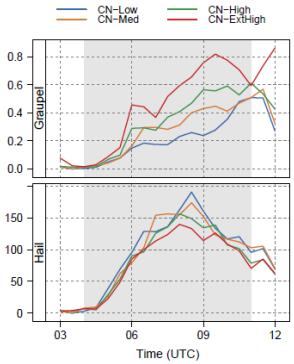

Figure 3.13: As in Figure 3.9, but for graupel and hail mixing ratios.

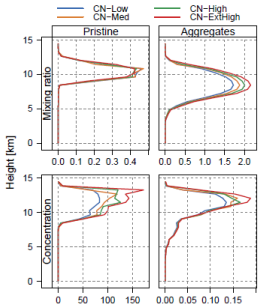

Figure 3.12: As in Figure 3.10, but for pristine and aggregate categories.

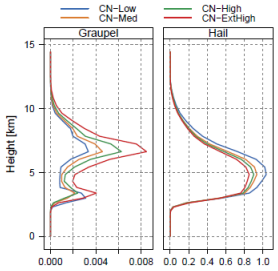

Figure 3.14: As in Figure 3.10, but for graupel and hail mixing ratios.

The experiments reveal a link between CCN number concentration and MCS's dynamics, where stronger downdrafts were observed under higher amounts of aerosols, generating more updraft cells in response. Moreover, the

Camponogara, G., Silva Dias, M. A. F., and Carrió, G. G.: Relationship between Amazon biomass burning aerosols and rainfall over the La Plata Basin, Atmos. Chem. Phys., 14, 4397-4407, 2014.

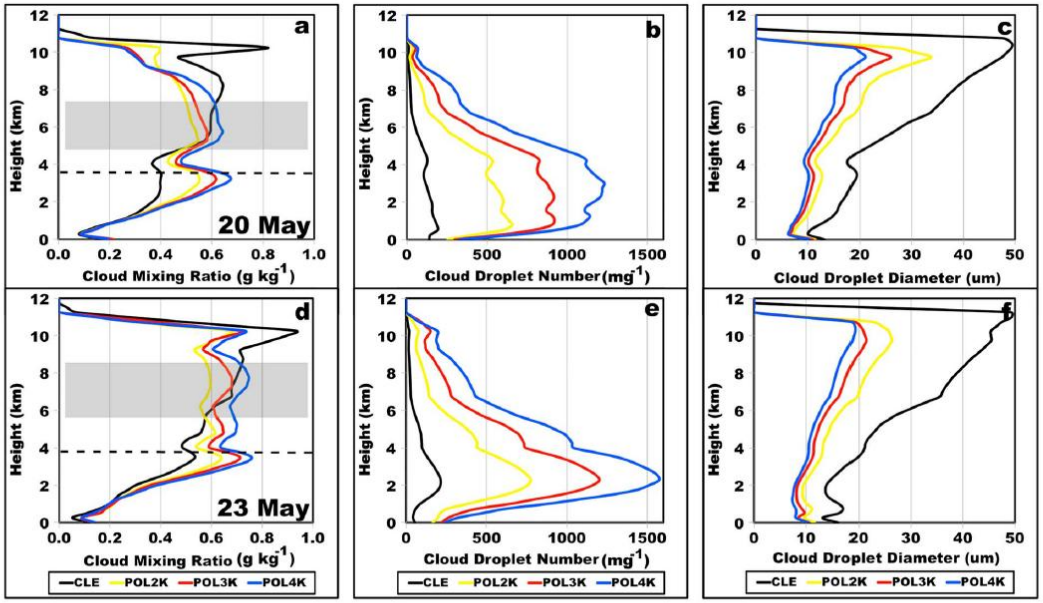

Figure 4. (a,d) Cloud droplet mixing ratio (g kg^{-1}), (b, e) number concentration (mg^{-1}), and (c, f) mean diameter (μm) for the 20 May (Figures 4a–4c) and 23 May (Figures 4d–4f) cases. Shaded areas indicate the elevation zone inclusive of the cloud water trend reversal relative to CLE. The freezing levels are denoted by the horizontal dashed lines.

Analyses indicate that for an increase in aerosol concentration from a clean continental to a highly polluted state, there was an increase in the rime collection rate of cloud water, which led to less lofted cloud water. Aerosol-induced trends in the cloud mixing ratio profiles were, however, nonmonotonic in the mixed phase region, such that a moderate increase in aerosol concentration produced the greatest reduction in cloud water.

Saleeby, S. M., S. C. van den Heever, P. J. Marinescu, S. M. Kreidenweis, and P. J. DeMott (2016), Aerosol effects on the anvil characteristics of mesoscale convective systems, J. Geophys. Res. Atmos., 121, 10,880–10,901, doi:10.1002/2016JD025082.

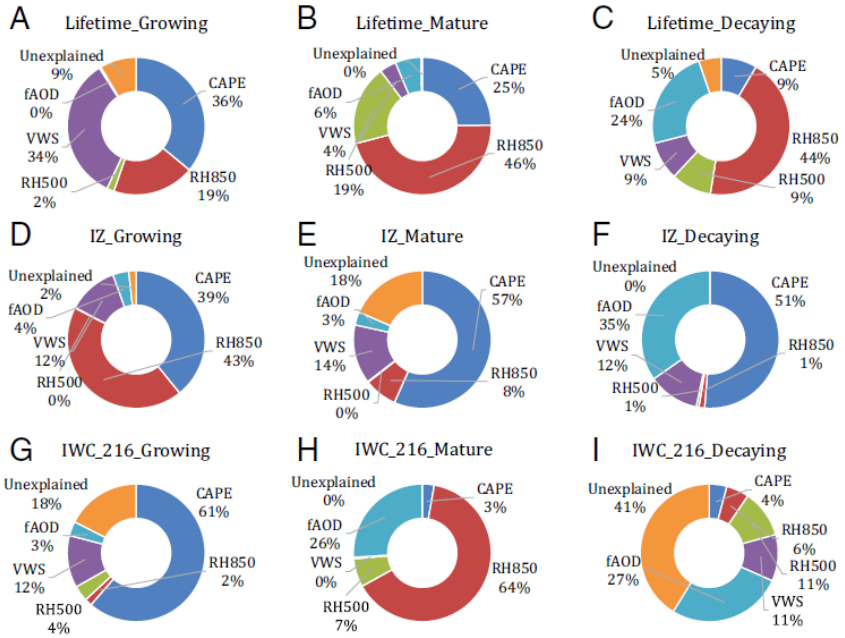

Fig. 2. Fraction of the total variance of the MCS's lifetime (*A*–*C*), IZ (*D*–*F*), and IWC_216 (*G*–*I*) explained by the environmental variables based on the multiple linear regression during the growing (*A*, *D*, and *G*), mature (*B*, *E*, and *H*), and decaying (*C*, *F*, and *I*) phases of the MCSs.

Our results show that MCSs' lifetime increases by 3–24 h when vertical wind shear (VWS) and convective available potential energy (CAPE) are moderate to high and ambient aerosol optical depth (AOD) increases by 1 SD (1σ). However, this influence is not as strong as that of CAPE, relative humidity, and VWS, which increase MCSs' lifetime by 3–30 h, 3–27 h, and 3–30 h per 1σ of these variables and explain up to 36%, 45%, and 34%, respectively, of the variance of the MCSs' lifetime. AOD explains up to 24% of the total variance of MCSs' lifetime during the decay phase. This result is physically consistent with that of the variation of the MCSs' ice water content (IWC) with aerosols, which accounts for 35% and 27% of the total variance of the IWC in convective cores and anvil, respectively, during the decay phase. The effect of aerosols on MCSs' lifetime varies between different continents. AOD appears to explain up to 20–22% of the total variance of MCSs' lifetime over equatorial South America compared with 8% over equatorial Africa. Aerosols over the Indian Ocean can explain 20% of total variance of MCSs' lifetime over South Asia because such MCSs form and develop over the ocean. These regional differences of aerosol impacts may be linked to different meteorological conditions.

Sudip Chakraborty, Rong Fu, Steven T. Massie, and Graeme Stephens. Relative influence of meteorological conditions and aerosols on the lifetime of mesoscale convective systems. PNAS July 5, 2016 113 (27) 7426-7431; first published June 16, 2016 https://doi.org/10.1073/pnas.1601935113

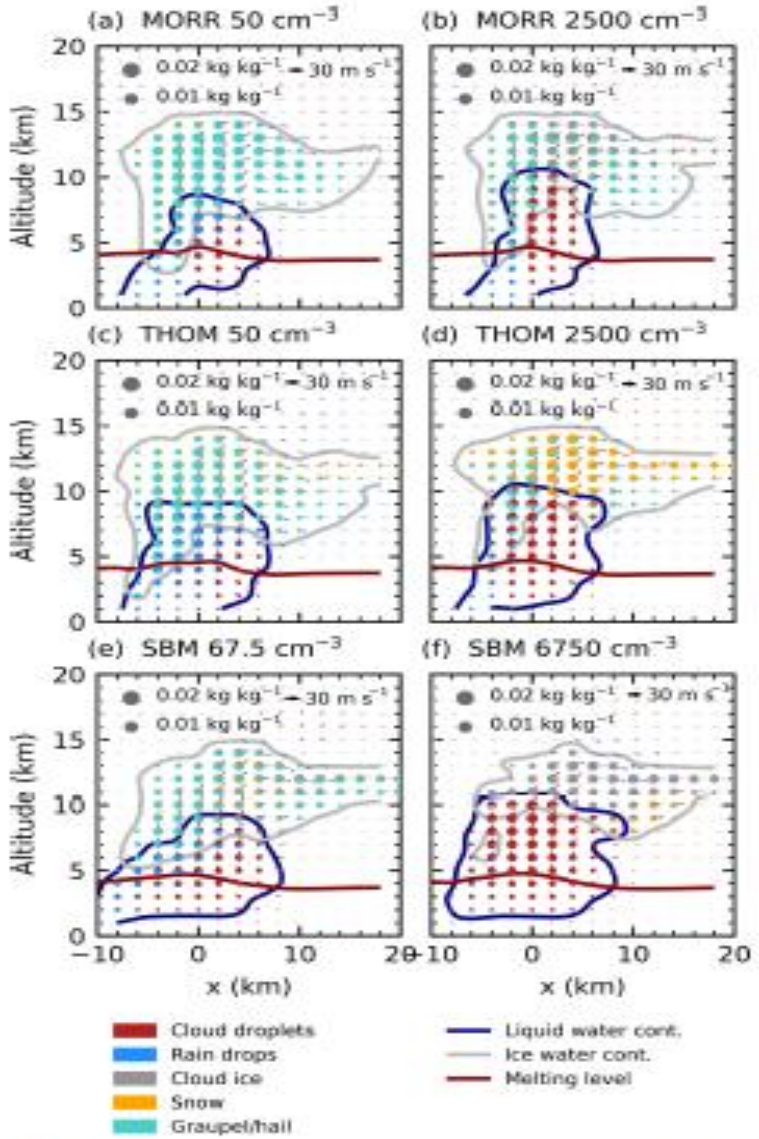

Figure 5. Hydrometeor mass mixing ratios in a slice along the line of travel of the cell for the cleanest (**a, c, e**) and most polluted (**b, d, f**) simulations after 60 min of simulation for the three microphysics schemes in CASE1.

This analysis confirms an expected decrease in warm rain formation processes due to autoconversion and accretion for more polluted conditions.

There is no evidence of a significant increase in the total amount of latent heat,

These changes in the microphysical processes explain some of the response in cloud mass and the altitude of the cloud centre of gravity.

However, there remain some contrasts in the development of the bulk cloud parameters between the microphysics schemes and the two simulated cases.

Heikenfeld, M., White, B., Labbouz, L., and Stier, P.: Aerosol effects on deep convection: the propagation of aerosol perturbations through convective cloud microphysics, Atmos. Chem. Phys., 19, 2601-2627, 2019.

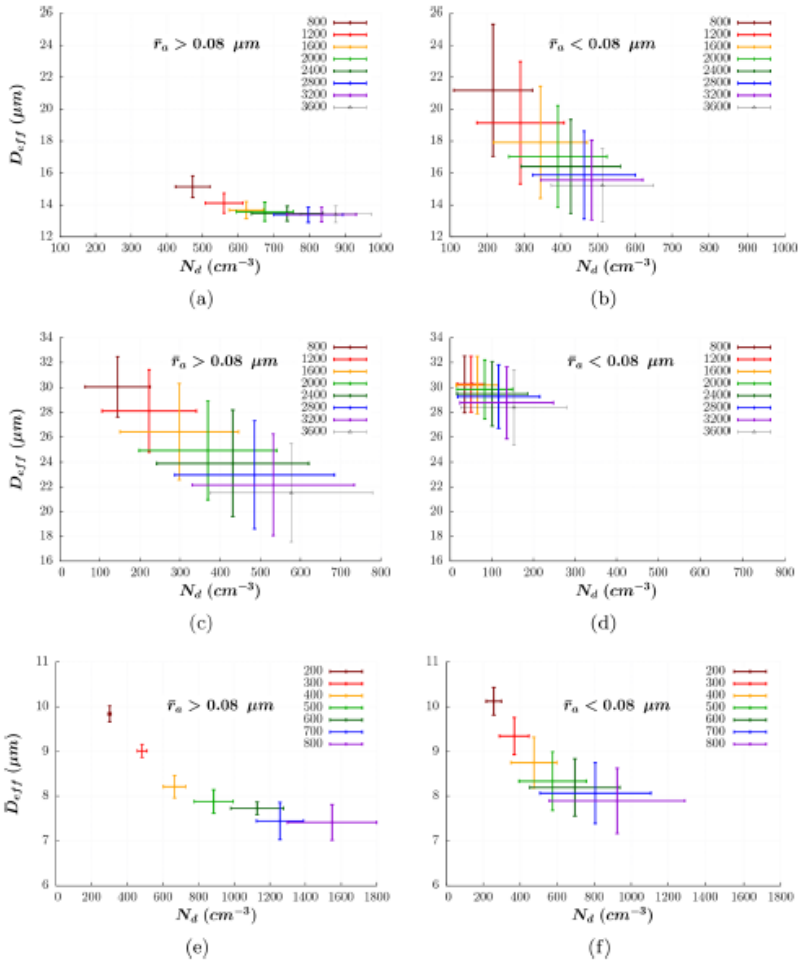

Figure 10. Mean and standard deviation of $\overline{N}_d$ and $\overline{D}_{eff}$ at cloud top from the simulations with entrainment and bins for the aerosols **(a, b)**, without entrainment **(c, d)** and without bins for the aerosol **(e, f)**.

Hernández Pardo, L., Toledo Machado, L. A., Amore Cecchini, M., and Sánchez Gácita, M.: Quantifying the aerosol effect on droplet size distribution at cloud top, Atmos. Chem. Phys., 19, 7839-7857, https://doi.org/10.5194/acp-19-7839-2019, 2019.

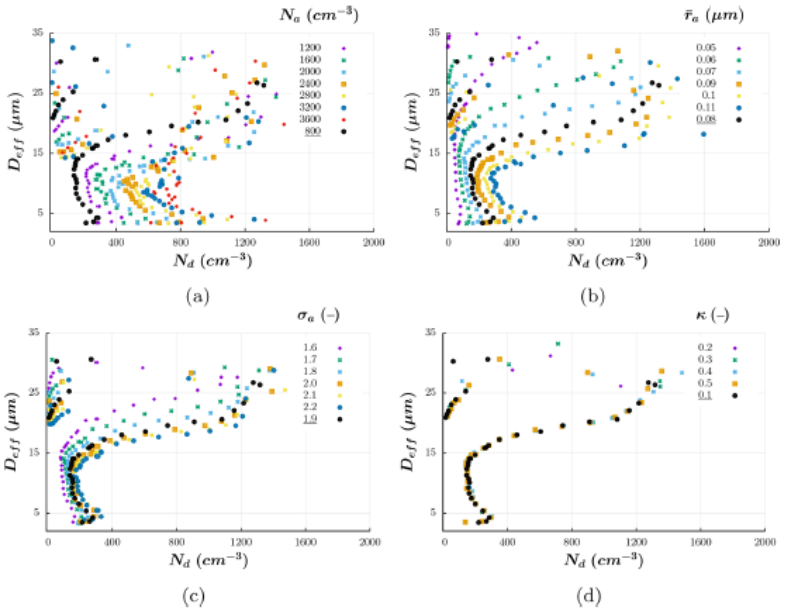

Figure 3. Illustration of the sensitivity of cloud top bulk properties to **(a)** the aerosol number concentration (cm^{-3}), **(b)** the median radius of the PSD (μm), **(c)** the geometric standard deviation of the PSD (–) and **(d)** the aerosol hygroscopicity (–). The markers represent the averaged DSDs for the time steps when the cloud top remains at the same model level during its growth. The colors distinguish between simulations using different values of the parameter specified at the top of the graphs. The control simulation is represented by black markers in the figures.

$$S_Y(X_i) = \frac{\partial \ln Y}{\partial \ln X_i}\Big|_{X_k},$$

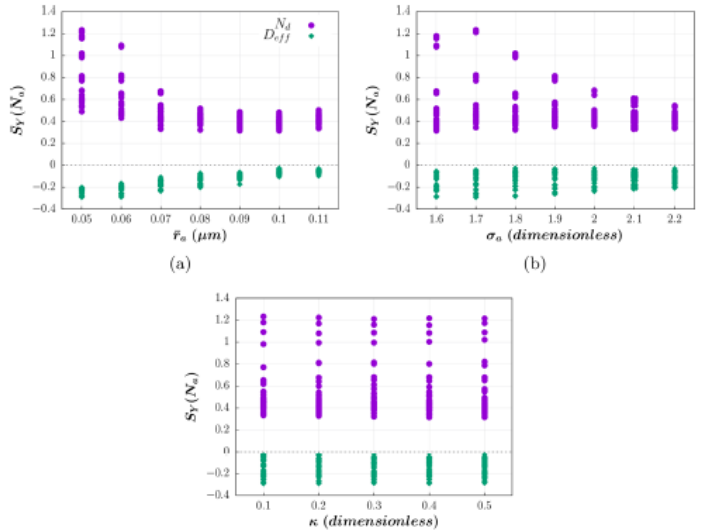

Figure 4. Sensitivities of the droplet number concentration and effective diameter to the aerosol number concentration, $S_Y(N_a)$, as a function of **(a)** the median radius of the PSD (μm), **(b)** the geometric standard deviation of the PSD (–) and **(c)** the aerosol hygroscopicity (–).

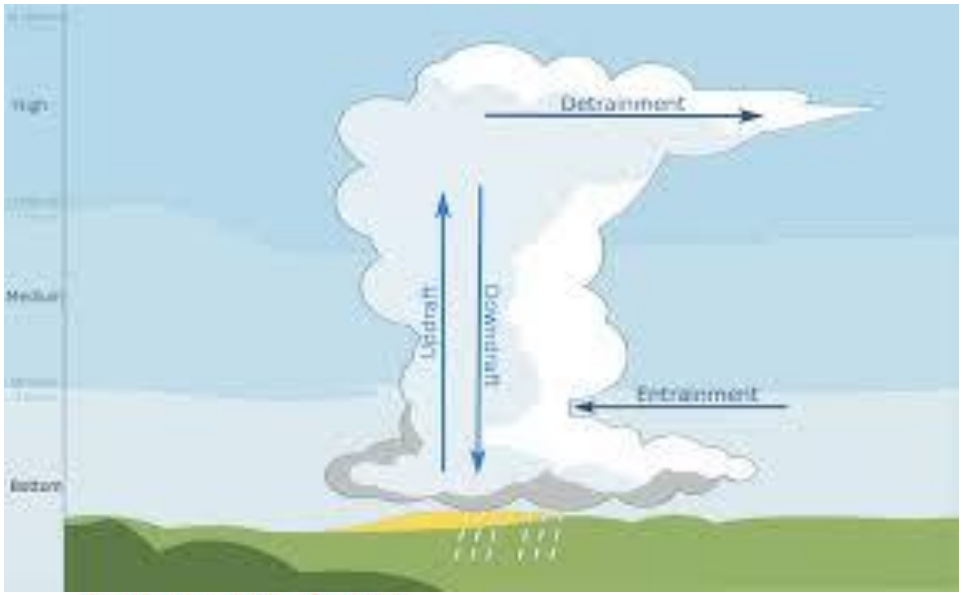

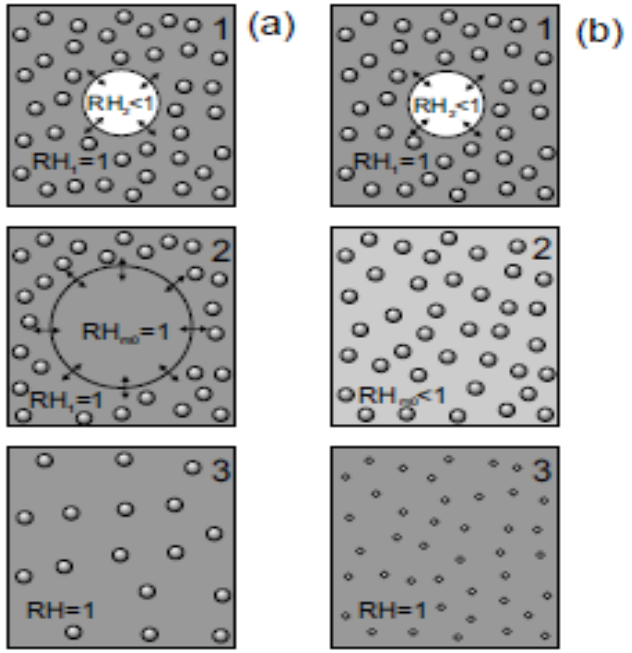

Figure 1. Classical conceptual diagram of **(a)** inhomogeneous and **(b)** homogeneous mixing. 1 – initial state; 2 – mixing state; 3 – final state.

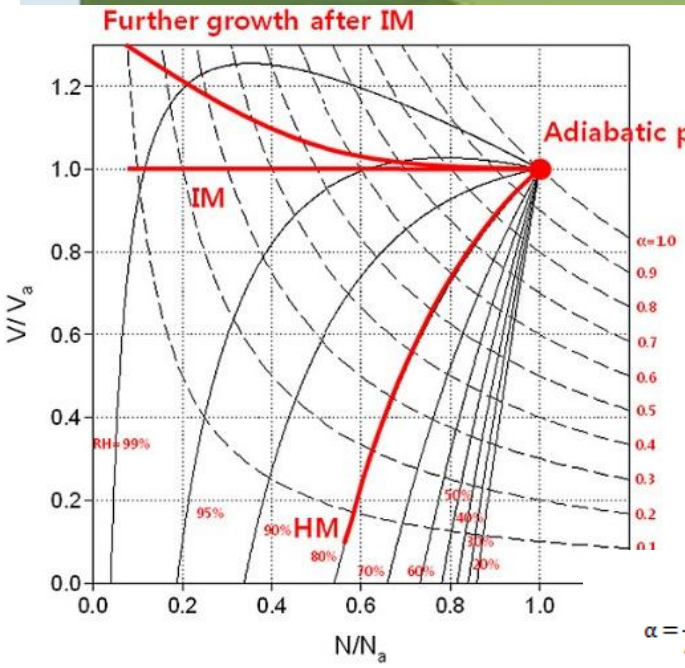

$$\alpha = \frac{L}{L_a} = \frac{(\pi/6)\rho_w NV}{(\pi/6)\rho_w N_a V_a} = \left(\frac{N}{N_a}\right)\left(\frac{V}{V_a}\right)$$

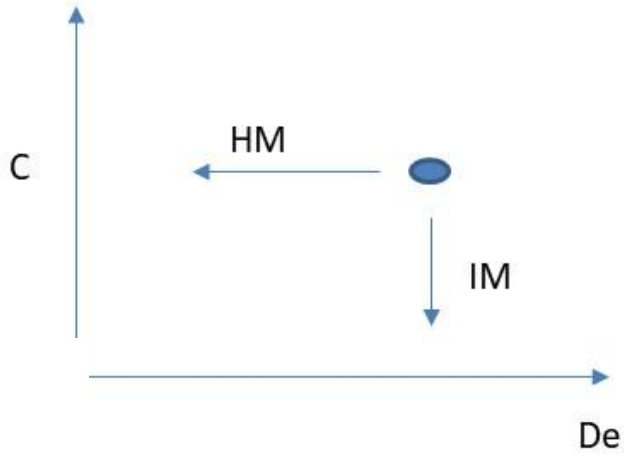

Korolev, A., Khain, A., Pinsky, M., and French, J.: Theoretical study of mixing in liquid clouds – Part 1: Classical concepts, Atmos. Chem. Phys., 16, 9235-9254, 2016.

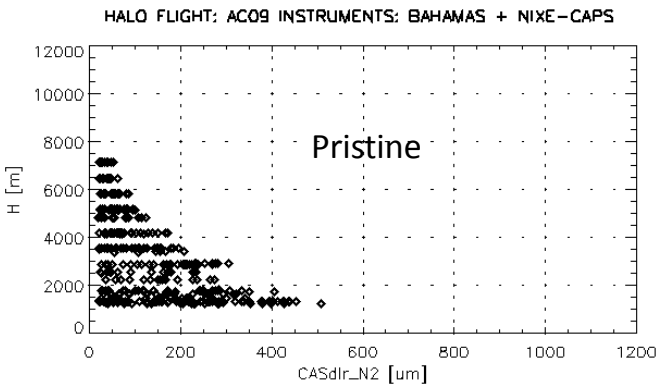

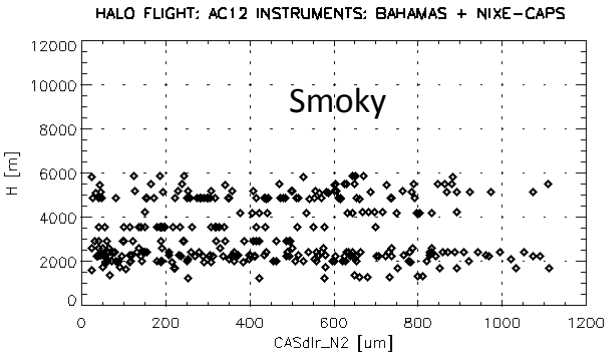

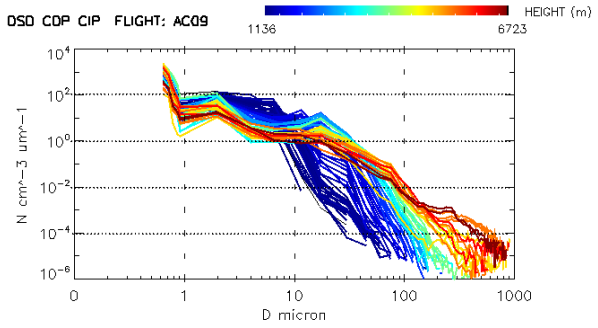

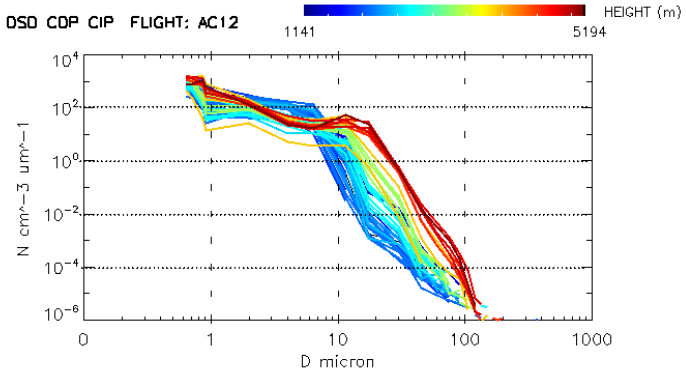

The ACRIDICON–CHUVA campaign to study tropical deep convective clouds and precipitation using the new German research aircraft HALO by Manfred Wendisch, Ulrich P¨oschl, Meinrat O. Andreae , Luiz A. T. Machado , Rachel Albrecht ¶, Hans Schlager k, Daniel Rosenfeld et al. - submitted– Bulletin of American Met. Soc.

Manaus pollution plume in the warm rain formation

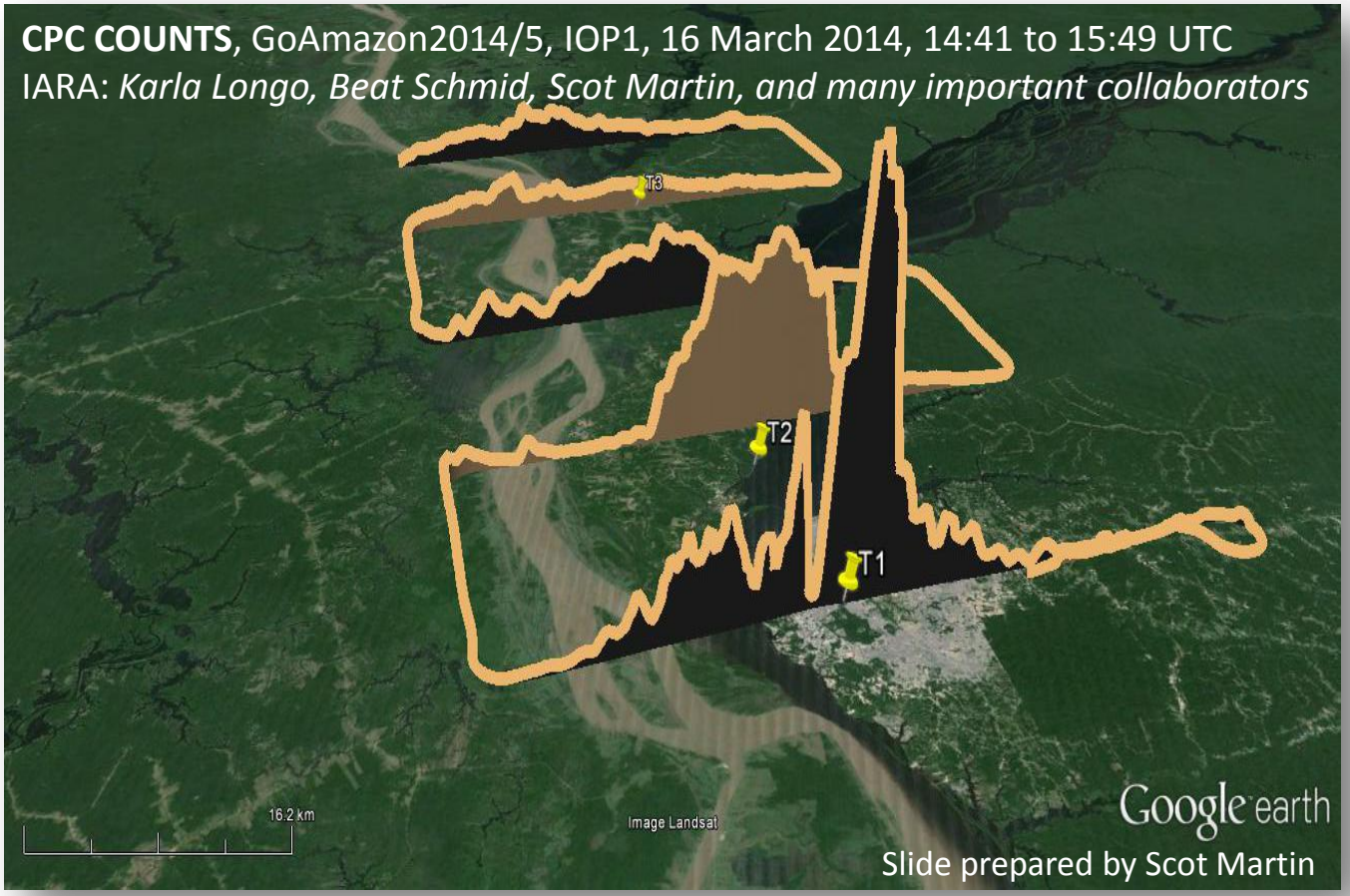
CPC COUNTS, GoAmazon2014/5, IOP1, 16 March 2014, 14:41 to 15:49 UTC
IARA: *Karla Longo, Beat Schmid, Scot Martin, and many important collaborators*
T3
T2
T1
16.2 km
Image Landsat
Google earth
Slide prepared by Scot Martin

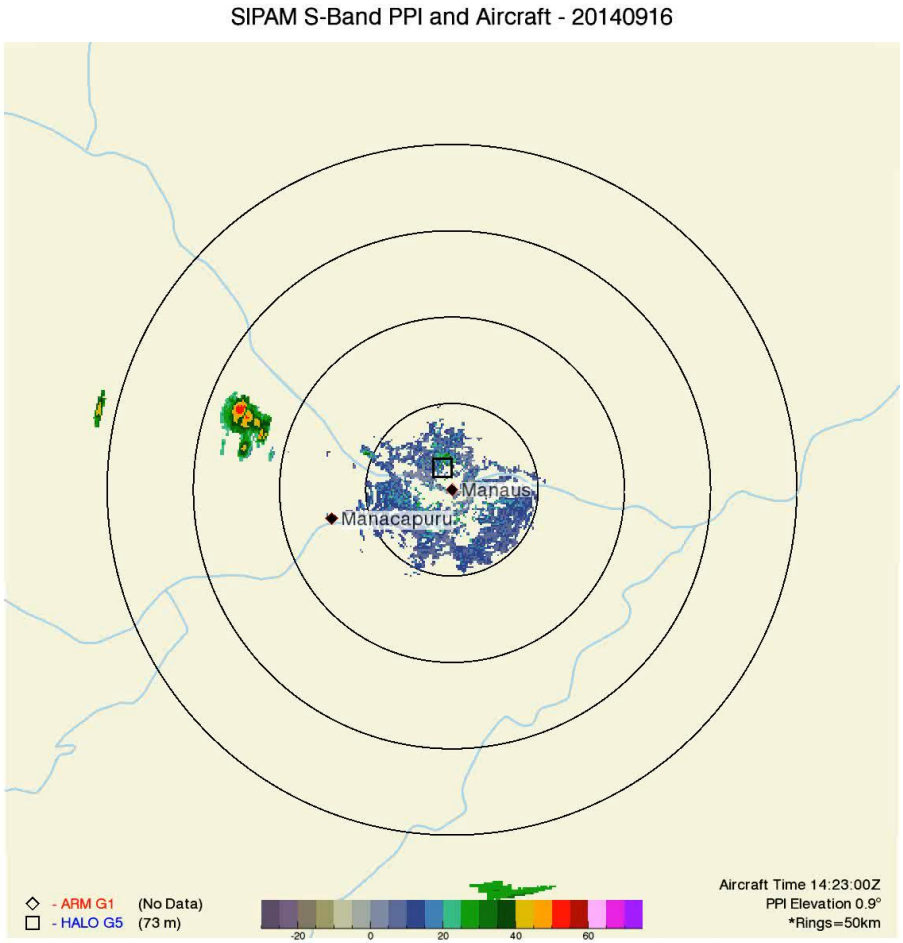
SIPAM S-Band PPI and Aircraft - 20140916
Manaus
Manacapuru
- ARM G1 (No Data)
- HALO G5 (73 m)
-20
0
20
40
60
Aircraft Time 14:23:00Z
PPI Elevation 0.9°
*Rings=50km

Manaus pollution plume in the warm rain formation

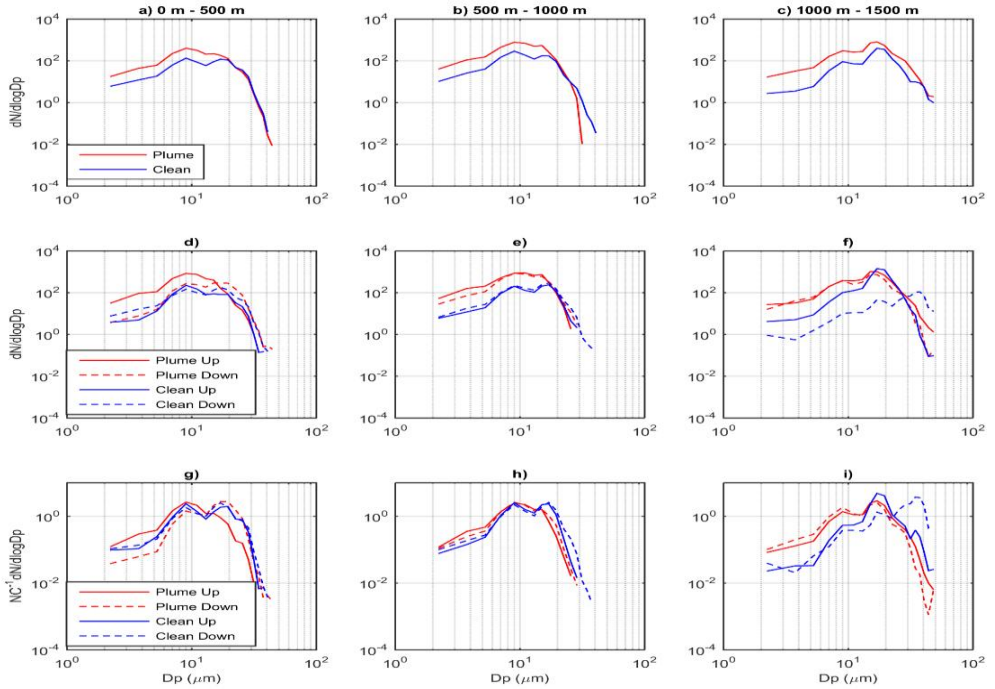

Mean DSDs for plume (red) or clean (blue) conditions as a function of altitude. Graphs a)-c) shows the mean DSDs in absolute number concentrations (cm^{-3}). d)-f) shows the mean DSDs for up- (w>1.5 m/s) and downdraft (w<-1.5 m/s) regions in cm^{-3}, while g)-i) show the NC-normalized ones.

Manaus' pollution plume impacts on cloud microphysical properties. Micael A. Cecchini[1], Luiz A.T. Machado[1], Jennifer M. Comstock[2], Fan Mei[2], John Schiling[2], Jian Wang[2], Jiwen Fan[2], Jason M. Tomlinson[2], Beat Schmid[2], Scot T. Martin[3]: Atmos. Chem. Phys. 2016

Manaus pollution plume in the warm rain formation

The wet season presents a clean background atmosphere characterized by frequent rain showers. The contrast between **background clouds** and those **affected by the Manaus pollution** can be observed and detailed. The **pollution-affected clouds** are found to have **smaller effective diameters and higher droplet number concentrations**. The differences range from **10 to 40 % for the effective diameter and are as high as 1000 % for droplet concentration** for the same vertical levels. The **growth rates of droplets with altitude are slower for pollution-affected clouds** This study shows that the pollution produced by Manaus significantly affects warm-phase microphysical properties of the surrounding clouds by changing the initial DSD formation.

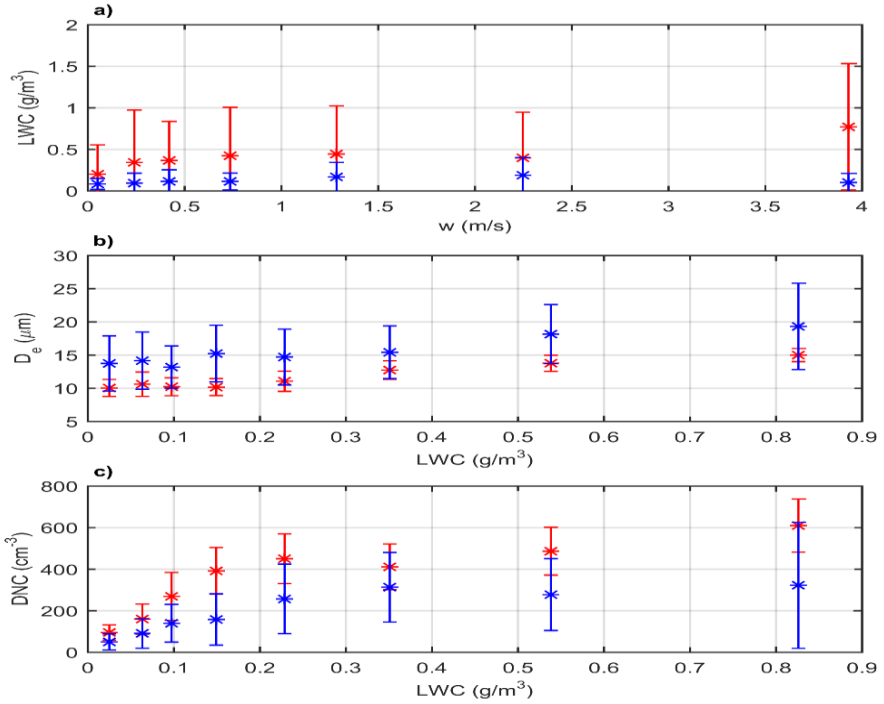

Manaus' pollution plume impacts on cloud microphysical properties. Micael A. Cecchini[1], Luiz A.T. Machado[1], Jennifer M. Comstock[2], Fan Mei[2], John Schiling[2], Jian Wang[2], Jiwen Fan[2], Jason M. Tomlinson[2], Beat Schmid[2], Scot T. Martin[3;] Atmos. Chem. Phys. 2016

Sensitivity of the updraft and aerosol concentration in the cloud processes

Particle concentration is the primary driver for the vertical profiles of effective diameter and droplet concentration in the warm phase of Amazonian convective clouds, while **updraft speeds have a modulating role in the total condensed water**. The DSD shape is crucial in understanding cloud sensitivities. The **aerosol effect on DSD shape was found to vary with altitude**, which can help models to better constrain the indirect aerosol effect on climate.

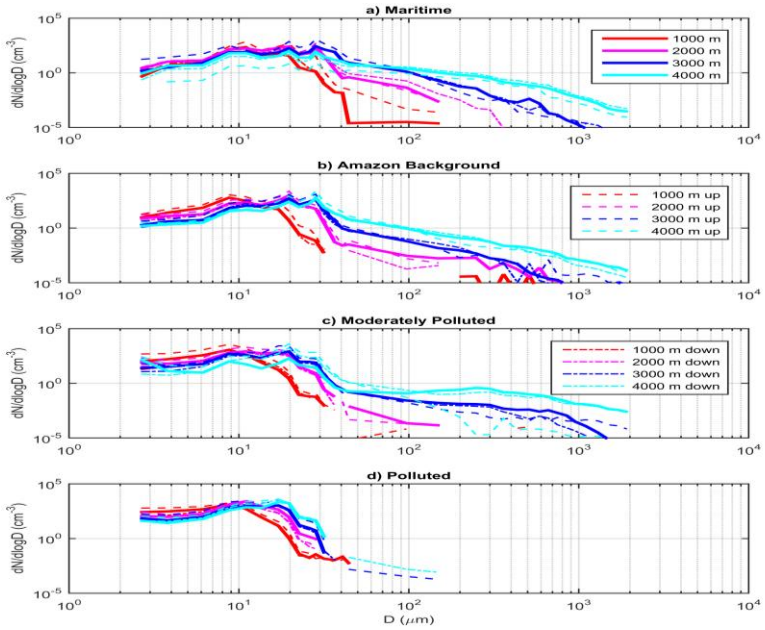

Droplet size distributions as function of altitude above cloud base, aerosol particle number concentration, and vertical wind speed, *W*. Four 1000-m-thick layers are considered in the vertical, where the legends in the graphs show the respective upper limit of each one. Solid lines represent averaged DSDs for -1 m s^{-1} ≤ *W* ≤ 1 m s^{-1}, i.e., for relatively neutral vertical movements. Dashed lines represent averaged DSDs for the updraft regions where *W* > 1 m s^{-1}, and dot-dashed lines represent the downdrafts (*W* < -1 m s^{-1}).

Cecchini, M. A., Machado, L. A. T., Andreae, M. O., Martin, S. T., Albrecht, R. I., Artaxo, P., Barbosa, H. M. J., Borrmann, S., Fütterer, D., Jurkat, T., Mahnke, C., Minikin, A., Molleker, S., Pöhlker, M. L., Pöschl, U., Rosenfeld, D., Voigt, C., Weinzierl, B., and Wendisch, M.: **Sensitivities of Amazonian clouds to aerosols and updraft speed**, Atmos. Chem. Phys., 17, 10037-10050, https://doi.org/10.5194/acp-17-10037-2017, 2017.

Sensitivity of the updraft and aerosol concentration in the cloud processes

Rainfall and Cloud Microphysics as Function of the Aerosol

Several Halo Cloud Profiles
(AC 7,8,9,11,12,13,14,18,19,20)
Only bellow melting layer

$$dlnD_0 \propto \left.\frac{dlnD_0}{dlnCN}\right|_{w,H} + \left.\frac{dlnD_0}{dlnw}\right|_{CN,H} + \left.\frac{dlnD_0}{dlnH}\right|_{CN,w}$$

	$\overline{S_{N_d}}$ (Cloud Droplet Concentration)	$\overline{S_{D_{eff}}}$ (Cloud Droplet Diameter)
N_a (Aerosol Concentration)	0.83 ± 0.21 R^2 = 0.91	-0.26 ± 0.074 R^2 = 0.89
w (Vertical Motion)	0.43 ± 0.28 R^2 = 0.81	0.03 ± 0.05 R^2 = 0.46
H (Height inside the cloud)	-0.14 ± 0.16 R^2 = 0.38	0.27 ± 0.05 R^2 = 0.93

Vertical bars indicate which variables are considered constant in the derivatives.

The first term on the right hand side represents the variations observed in the mean volumetric diameter due to changes in Aerosol Concentration with similar w and H conditions.

As the derivatives are considered under the natural logarithm, the results are normalized and can be directly quantitatively compared.

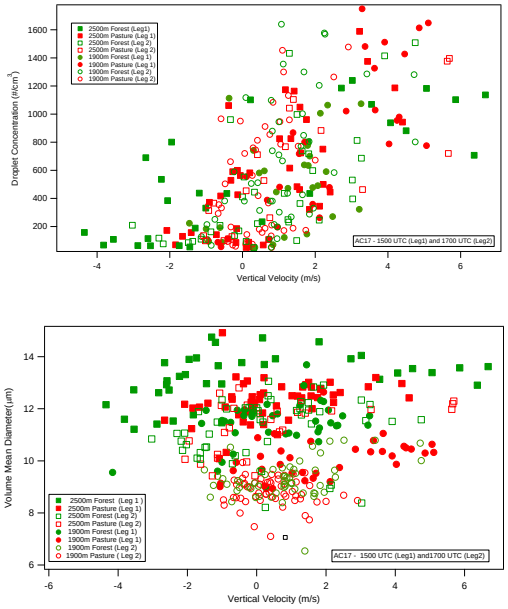

HALO Flight AC17 Forest – Deforested areas – same level nearly same time. Cloud droplet concentration and diameter as function the vertical velocity at different Height

Sensitivity of the updraft and aerosol concentration in the cloud processes

$$S_{N_d}(N_a) = \left.\frac{\partial \ln N_d}{\partial \ln N_a}\right|_{w,H}, S_{N_d}(w) = \left.\frac{\partial \ln N_d}{\partial \ln w}\right|_{N_a,H}, S_{N_d}(H) = \left.\frac{\partial \ln N_d}{\partial \ln H}\right|_{w,N_a}$$

	$\overline{S_{N_d}}$	$\overline{S_{D_{eff}}}$
N_a	**0.84** ± 0.21	**-0.25** ± 0.074
	R^2 = 0.91	R^2 = 0.89
w	**0.43** ± 0.28	**0.028** ± 0.058
	R^2 = 0.81	R^2 = 0.46
H	**-0.13** ± 0.16	**0.28** ± 0.058
	R^2 = 0.38	R^2 = 0.93

An increase of **100% in aerosol concentration** results in an **84% increase in droplet number concentration** and the **effective droplet diameter decreases 25%.**

An increase of **100% in updraft wind speed** results in an **43% increase in droplet number concentration** and the **effective droplet diameter is** nearly unchanged

Aerosol concentration is the primary driver for DSD, whereas the updrafts mainly affect droplet number concentration and liquid water content.

Cecchini, M. A., Machado, L. A. T., Andreae, M. O., Martin, S. T., Albrecht, R. I., Artaxo, P., Barbosa, H. M. J., Borrmann, S., Fütterer, D., Jurkat, T., Mahnke, C., Minikin, A., Molleker, S., Pöhlker, M. L., Pöschl, U., Rosenfeld, D., Voigt, C., Weinzierl, B., and Wendisch, M.: **Sensitivities of Amazonian clouds to aerosols and updraft speed**, Atmos. Chem. Phys., 17, 10037-10050, https://doi.org/10.5194/acp-17-10037-2017, 2017.

Sensitivity of the updraft and aerosol concentration in the cloud processes

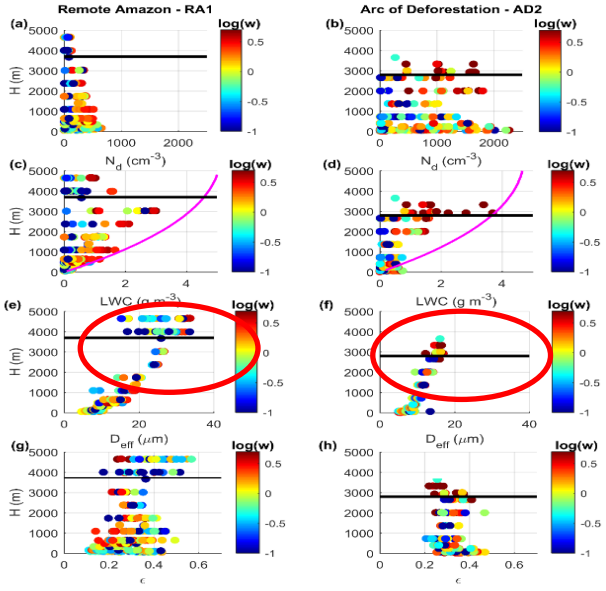

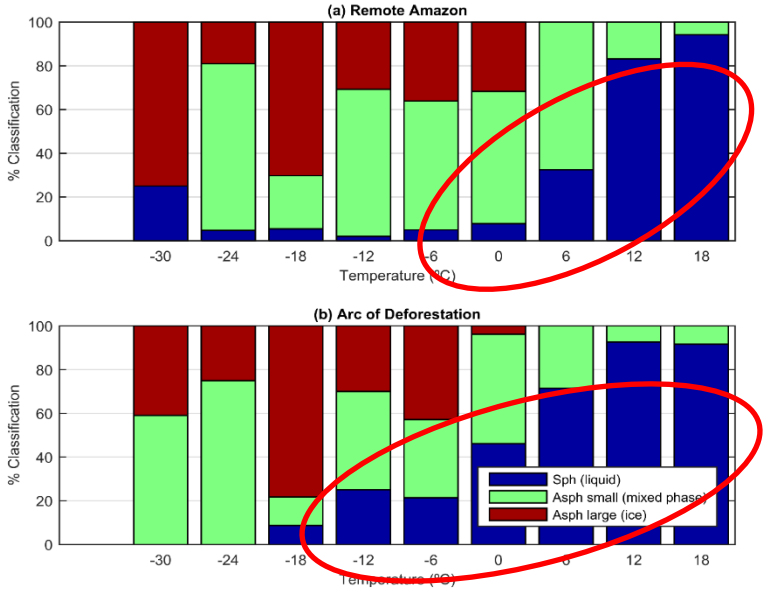

Illustration of microphysical processes in Amazonian deep convective clouds in the Gamma phase space: Introduction and potential applications Cecchini, M. A., Machado, L. A. T., Wendisch, M., Costa, A., Krämer, M., Andreae, M. O., Afchine, A., Albrecht, R. I., Artaxo, P., Borrmann, S., Fütterer, D., Klimach, T., Mahnke, C., Martin, S. T., Minikin, A., Molleker, S., Pardo, L. H., Pöhlker, C., Pöhlker, M. L., Pöschl, U., Rosenfeld, D., and Weinzierl, B.:, Atmos. Chem. Phys. Discuss., https://doi.org/10.5194/acp-2017-185, in review, 2017.

Frequency of occurrence of NIXE-CAPS sphericity classifications for (a) the remote Amazon and (b) the Arc of Deforestation. “Sph (liquid)” stands for many only spherical (D < 50 µm) and predominantly spherical (D > 50 µm) hydrometeors, “Asph small (mixed phase)” for many predominantly spherical (D < 50 µm) and only aspherical (D > 50 µm) hydrometeors, and “Asph large (ice)” for only very few aspherical (D < 50 µm) and only aspherical (D > 50 µm) hydrometeors. Temperatures shown on the x-axis are the center for 6 °C intervals, which corresponds to roughly 1-km-thick layers.

Convective Invigoration what is new?

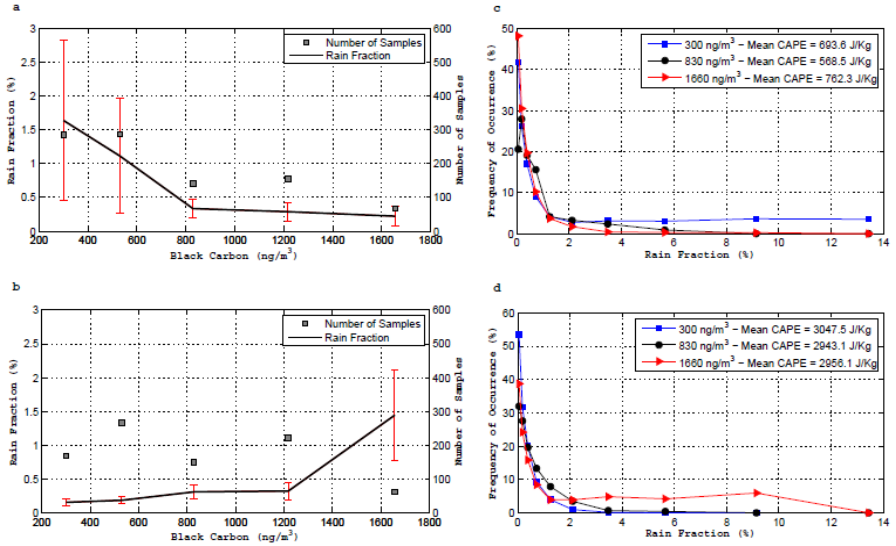

Figure 4. Mean, standard deviation, and number of samples of rain fraction (RF) for different black carbon (BC) concentrations for less unstable **(a)** and more unstable **(b)** atmospheres in the dry period. RF frequency histograms for the first, third, and fifth BC concentrations in **(a)** and **(b)**, are shown for less unstable **(c)** and more unstable **(d)** atmospheres. The first and third curves in **(c)** and **(d)** are significantly different as determined by a *t* test at the 95 % confidence level.

Gonçalves, W. A., Machado, L. A. T., and Kirstetter, P.-E.: Influence of biomass aerosol on precipitation over the Central Amazon: an observational study, Atmos. Chem. Phys., 15, 6789-6800, https://doi.org/10.5194/acp-15-6789-2015, 2015.

Convective Invigoration what is new?

Daniel Rosenfeld, *et al. Science* **321**, 1309 (2008)

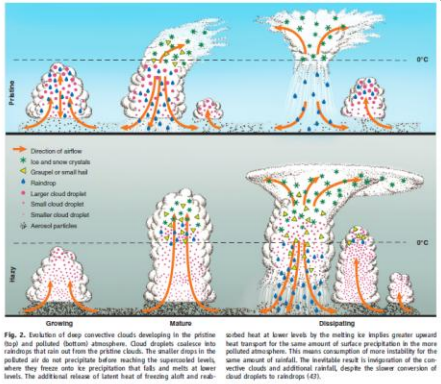

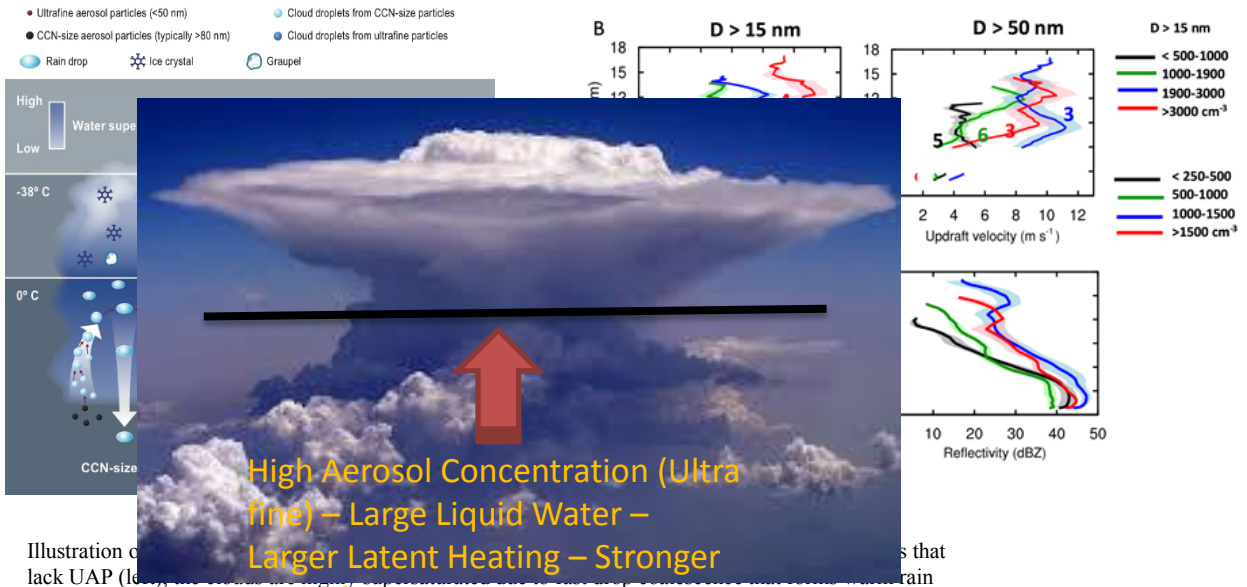

Substantial Convection and Precipitation Enhancements by Ultrafine Aerosol Particles Jiwen Fan[1*], Daniel Rosenfeld[2], Yuwei Zhang[1,3], Scott E. Giangrande[4], Zhanqing Li[3], Luiz A. T. Machado[5], Scot T. Martin[6], Yan Yang[1,7], Jian Wang[4], Henrique M. J. Barbosa[8], Jennifer M. Comstock[1], Zhe Feng[1], Wenhua Gao[1,9], Helber B. Gomes[10], Fan Mei[1], Rodrigo A. F. de Souza. Submitted to Science.

Illustration c s that lack UAP (le rain which reduces the integrated droplet surface area available for condensation. With added UAP (right), an additional number of cloud droplets are nucleated, which lowers supersaturation drastically by enhanced condensation, releasing additional latent heat at low and middle levels and intensifying convection. The additional condensate adds to both the warm rain and supercooled cloud water that (when freezing occurs aloft) further enhances convection (a small increase in rate, but enhances precipitation and storm electrification).

, that the grown nanoparticles enhance the vertical development of shallow warm clouds early in the cloud lifecycle, then augment the transition of shallow to deep convective clouds, with appreciable reductions in the effective cloud droplet sizes and rain rates. Our findings suggest that urban nanoparticles could rapidly grow in other environments as well due to relatively high abundance of SVOCs, and thereby exert substantial impacts on climate.

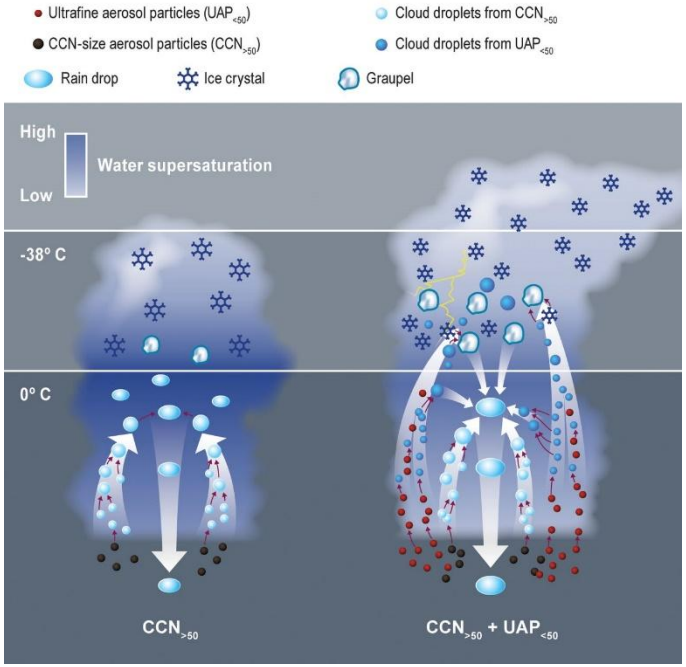

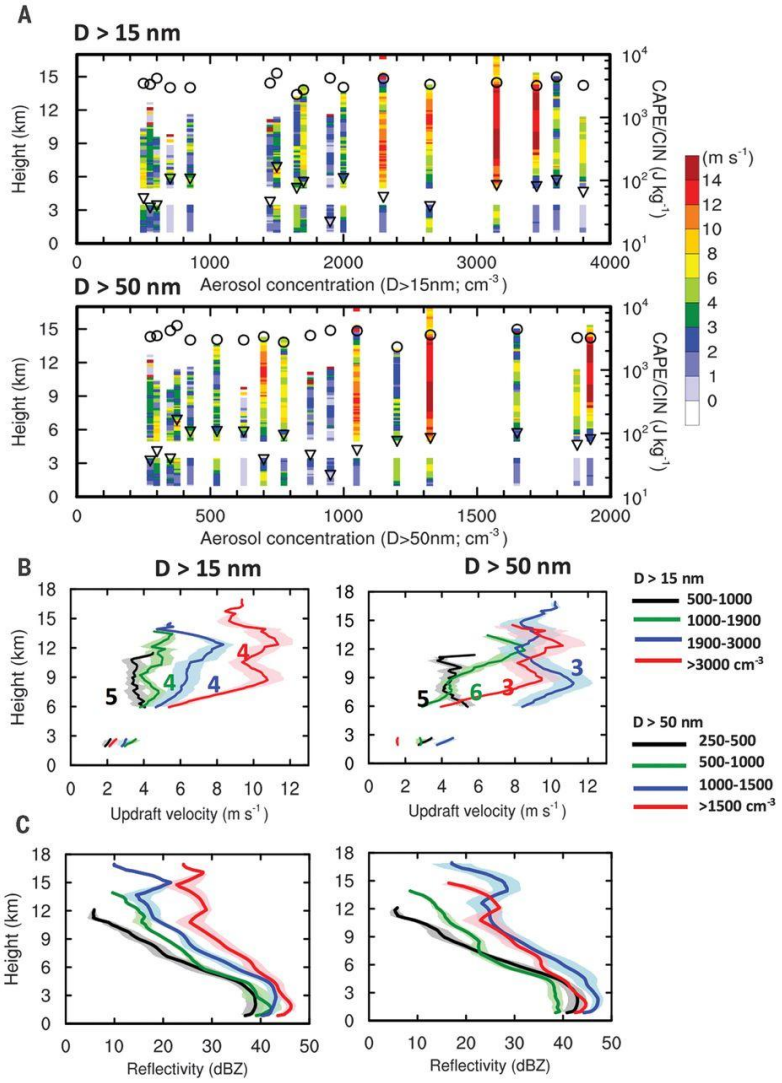

Aerosol –Cloud-Precipitation Interaction in the Gamma Space

Chuva – contribuição a Modelagem

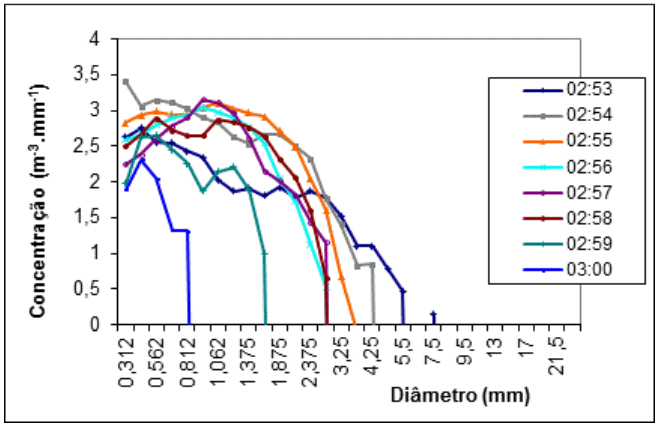

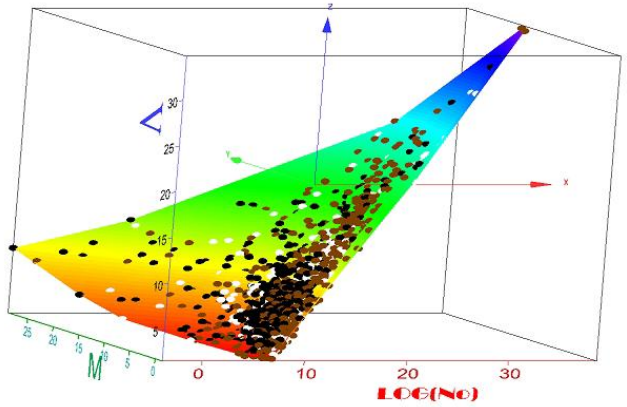

From cloud droplet mass mixing ratios (or De) and number concentrations →full size distribution

Função Gama

$$N(D) = N_o D^{\mu} \exp(-\Lambda D),$$

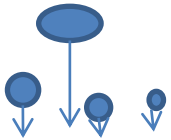

Processos de coleta, evaporação, velocidade terminal, etc

Aerosol –Cloud-Precipitation Interaction in the Gamma Space

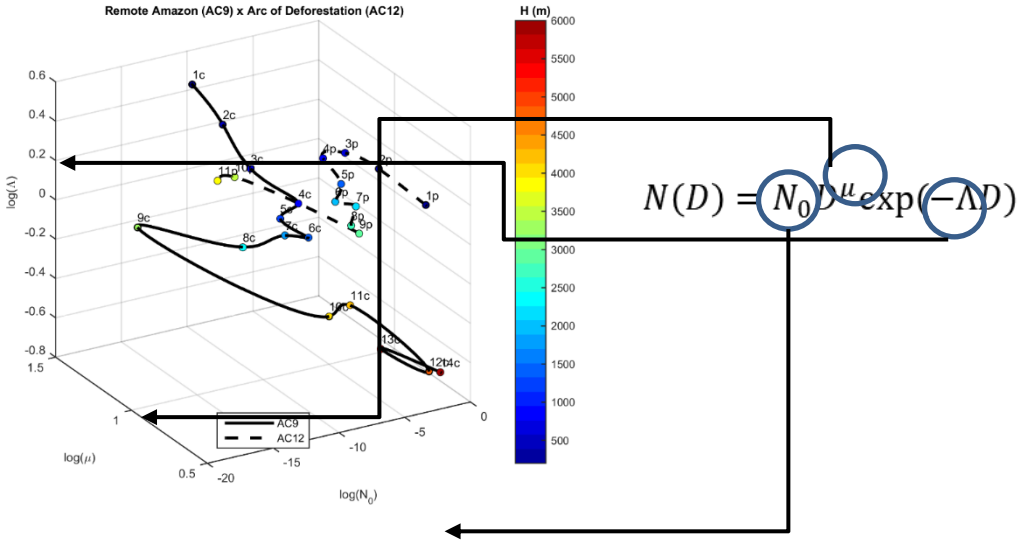

$$N(D) = N_0 D^{\mu} \exp(-\Lambda D)$$

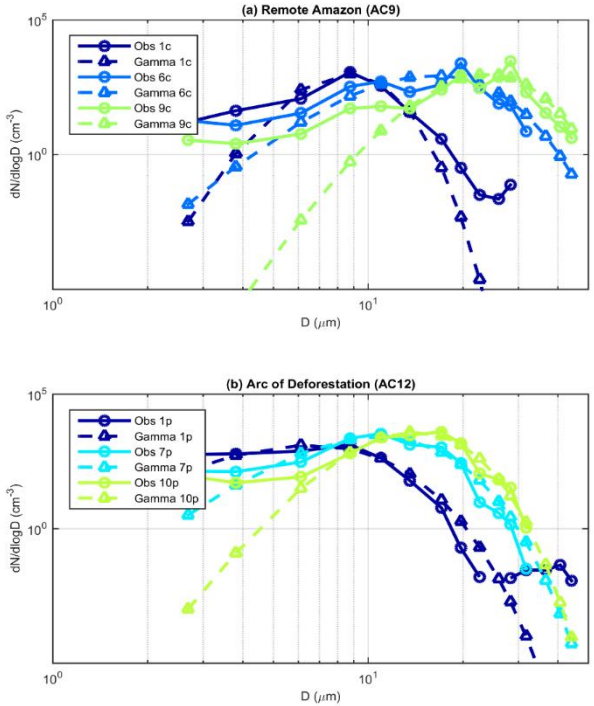

Aerosol –Cloud-Precipitation Interaction in the Gamma Space

Conceptual drawing of the properties of the Gamma phase space in the warm layer of the clouds. The dotted gray line represents one trajectory through the phase space, representing the DSD evolution. P_1 is one DSD that grows by condensation and collision-coalescence to reach P_2. The displacement represented by the pseudo-force $\vec{F}$ is decomposed into two components - $\overrightarrow{F_{cd}}$ **(condensational pseudo-force) and** $\overrightarrow{F_{cl}}$ **(collisional pseudo-force).** Also shown are the two DSDs representative of points P_1 and P_2.

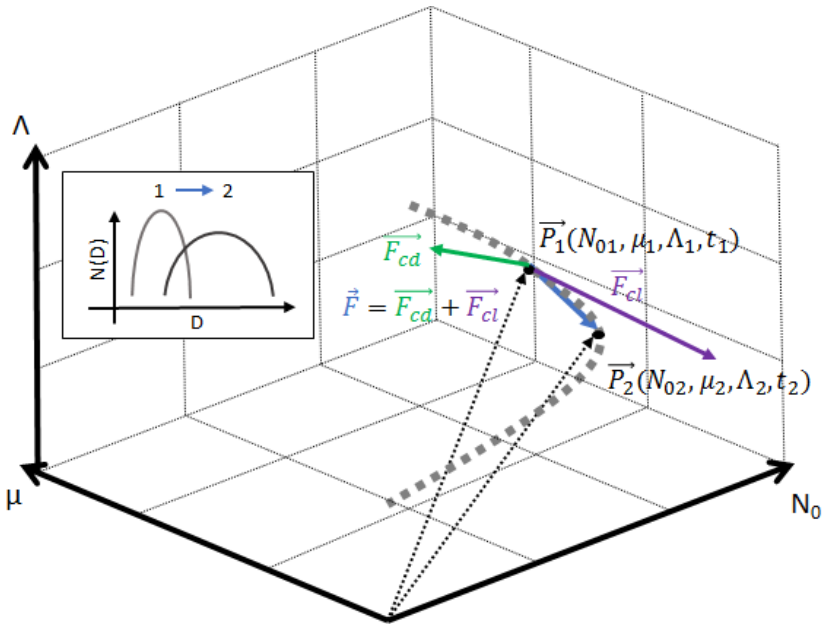

Illustration of microphysical processes in Amazonian deep convective clouds in the Gamma phase space: Introduction and potential applications Cecchini, M. A., Machado, L. A. T., Wendisch, M., Costa, A., Krämer, M., Andreae, M. O., Afchine, A., Albrecht, R. I., Artaxo, P., Borrmann, S., Fütterer, D., Klimach, T., Mahnke, C., Martin, S. T., Minikin, A., Molleker, S., Pardo, L. H., Pöhlker, C., Pöhlker, M. L., Pöschl, U., Rosenfeld, D., and Weinzierl, B.:, Atmos. Chem. Phys. Discuss., https://doi.org/10.5194/acp-2017-185, in review, 2017.

Aerosol –Cloud-Precipitation Interaction in the Gamma Space

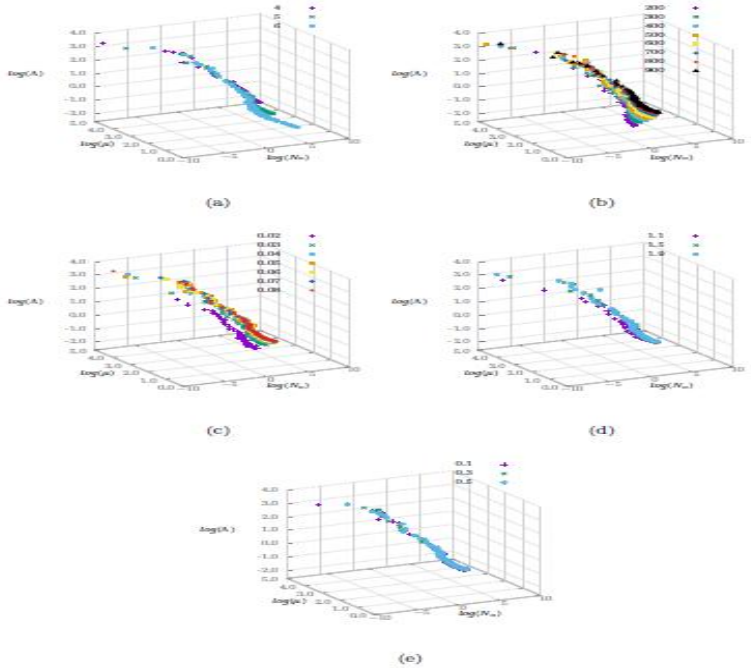

Figure 2: Sensitivity in the gamma-space to: a) updraft velocity, b) initial aerosol number concentration, c) mean size of the aerosol distribution, d) geometric standard deviation of the aerosol size distribution and e) aerosol hygroscopicity

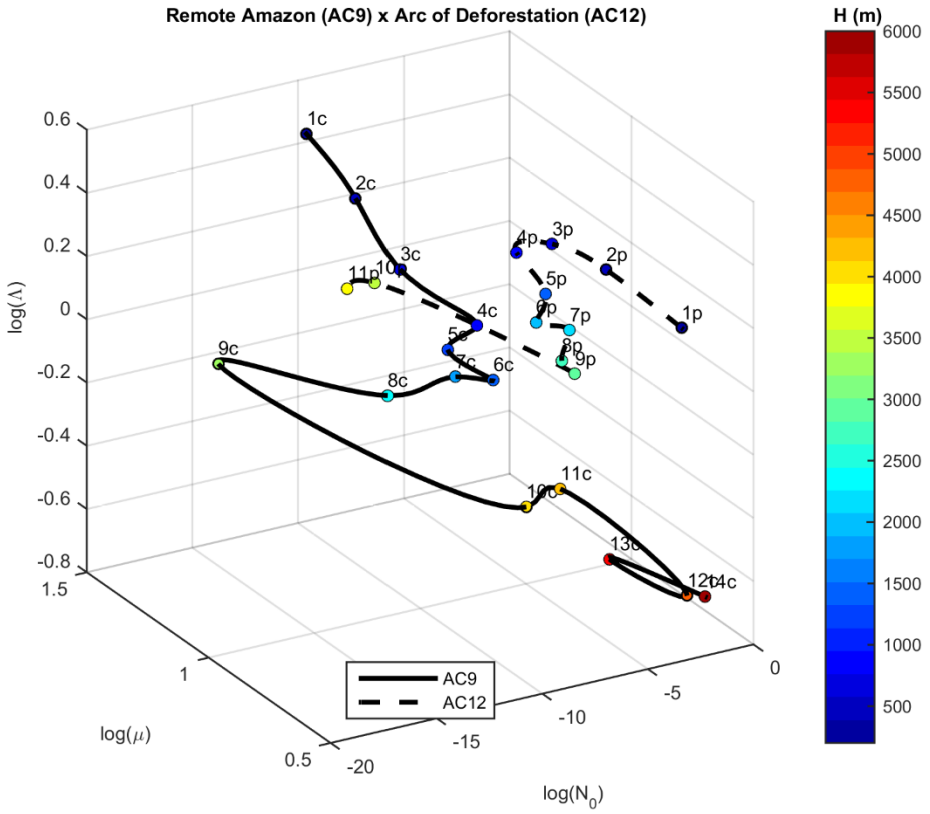
Remote Amazon (AC9) x Arc of Deforestation (AC12)
H (m)
6000
5500
5000
4500
4000
3500
3000
2500
2000
1500
1000
500
log(Λ)
0.6
0.4
0.2
0
-0.2
-0.4
-0.6
-0.8
log(μ)
1.5
1
0.5
log(N0)
0
-5
-10
-15
-20
AC9
AC12
1c
2c
3c
4c
5c
6c
7c
8c
9c
10c
11c
12c
13c
14c
1p
2p
3p
4p
5p
6p
7p
8p
9p
10p
11p

Aerosol –Cloud-Precipitation Interaction in the Gamma Space

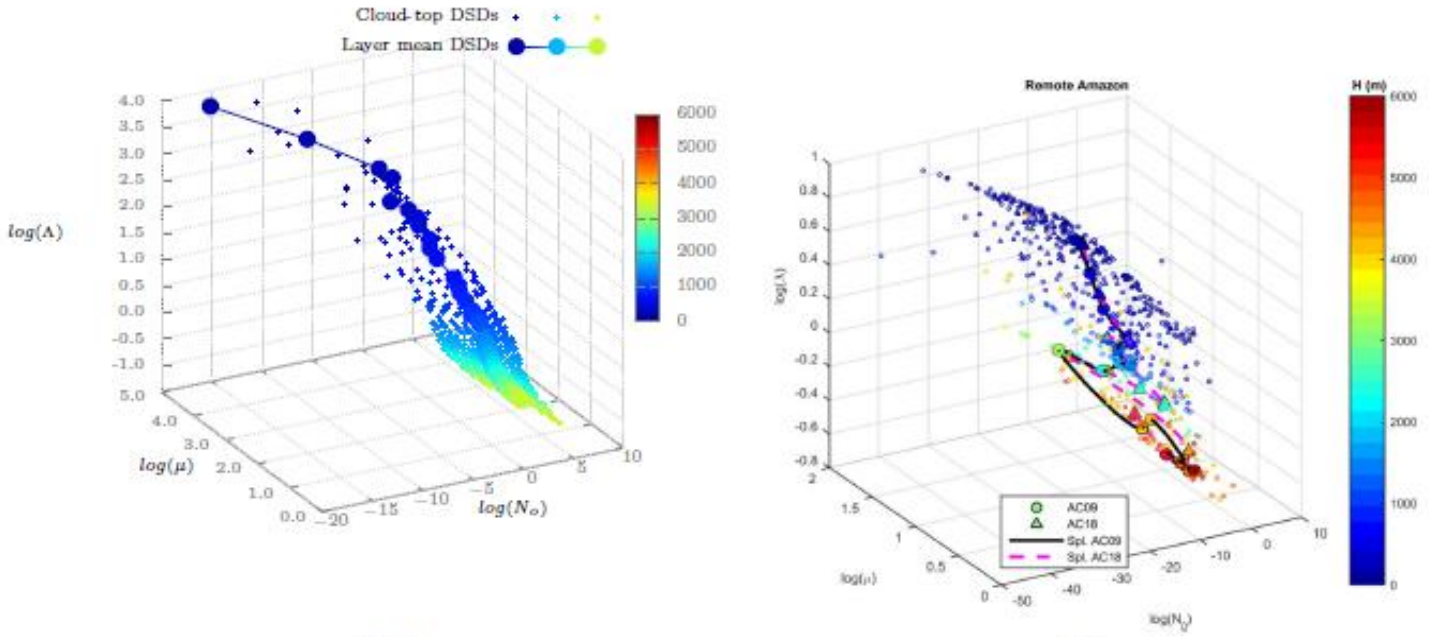

Column Bin Microphysics Model - Similarities between the model simulations and observations.

Figure 1:

Aerosol –Cloud-Precipitation Interaction in the Gamma Space

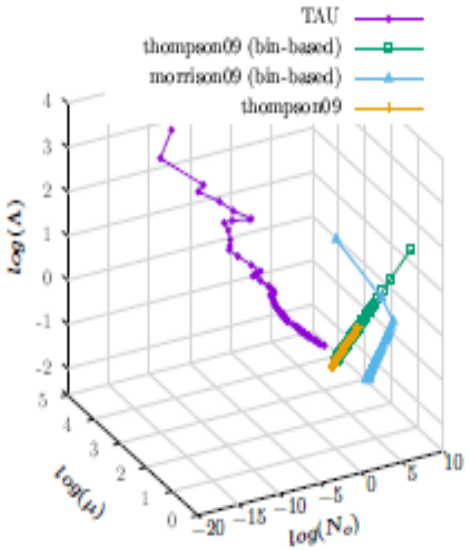

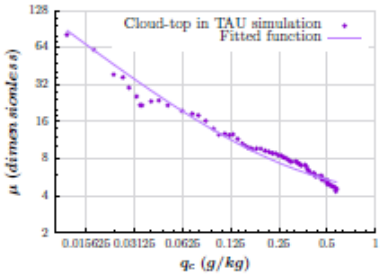

$$\mu(q_c) = \frac{1}{q_c} + \frac{1000}{N_d} + 2$$

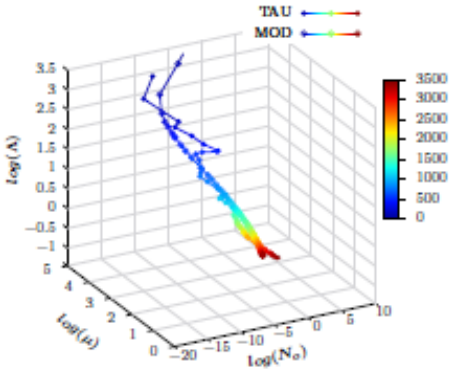

Aerosol –Cloud-Precipitation Interaction in the Gamma Space

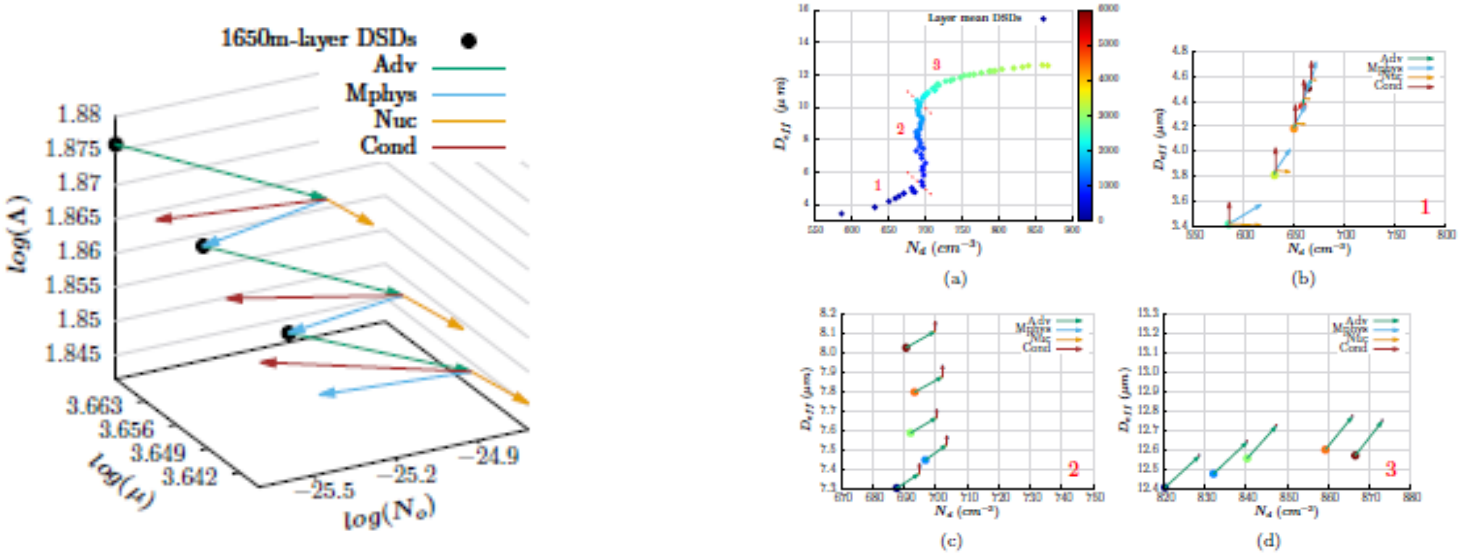

Cloud-top microphysics evolution in the Gamma phase-space from a modelling perspective. Lianet Hernández Pardo, Luiz Augusto Toledo Machado, and Micael Amore Cecchini. In submisson process to Atmos. Chem, and Physc., 2018

Cloud–aerosol interactions

- *First indirect effect*: Higher aerosol concentration produces more but smaller cloud droplets whose collective surface area is greater, making the cloud more reflective; a potentially significant negative climate forcing.
- *Second indirect effect*: Smaller droplets precipitate less, increasing cloud water content and lifetime; this has not yet been observationally verified and may be offset by faster evaporation of smaller droplets when dry air is entrained into the cloud.
- *Semi-direct effect*: Warming of air by solar absorption by lower albedo aerosols (e.g., black carbon) evaporates cloud droplets or affects atmospheric stability; cloud may increase or decrease depending on the type of cloud and altitude of the warming.

NE Pacific ship tracks

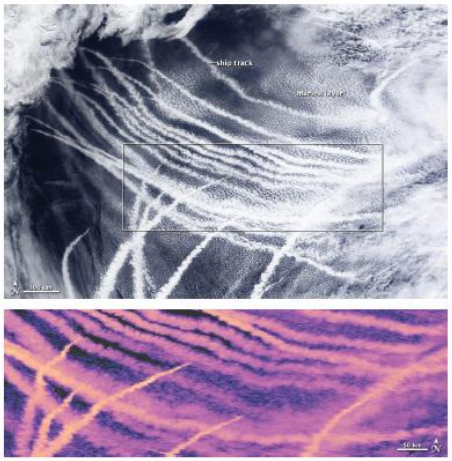

(images courtesy NASA)

Precipitation–aerosol interactions

- *Wet deposition (scavenging)*: Precipitating droplets collect aerosol particles and remove them from the atmosphere (below-cloud scavenging), or cloud droplets that form by nucleating onto an aerosol remove the aerosol when they rain out (in-cloud scavenging); this is the primary mechanism for removing aerosols from the atmosphere

- *Invigoration of convection*: Higher aerosol concentration limits coalescence growth of cloud droplets into rain drops in a convective updraft, allowing more liquid to be carried up to colder temperatures; the resulting increase in ice formation releases additional latent heat that strengthens the convection; this is currently a controversial hypothesis

Take-away messages

- Clouds form either because of convective instability or because of stable lifting of air masses; they are tracers of Earth's general circulation
- Convective clouds transport heat, moisture, momentum and produce much of Earth's precipitation; stratiform clouds produce some precipitation but dominate radiative effects
- Clouds with low and high tops play different roles in the climate system via how much precipitation they form and/or whether they influence primarily SW or LW radiation
- Cloud feedbacks in a changing climate are due to changes in cloud cover, height, optical thickness, phase, and location; some are well understood, others are not
- Interactions of aerosols with clouds affect cloud optical thickness, and potentially cloud cover and precipitation; many of these interactions are uncertain

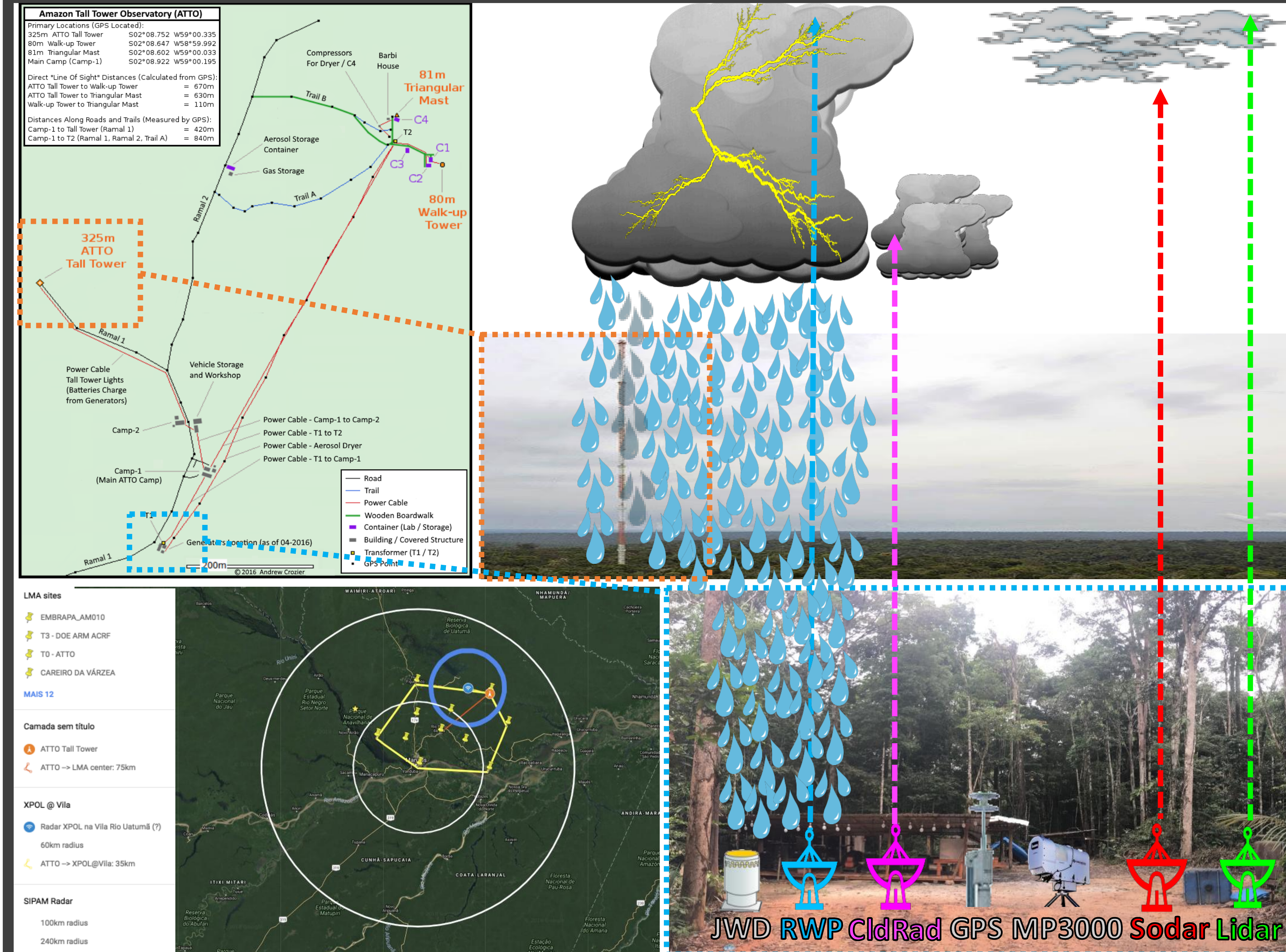

Amazon Tall Tower Observatory (ATTO)
Primary Locations (GPS Located):
325m ATTO Tall Tower S02°08.752 W59°00.335
80m Walk-up Tower S02°08.647 W58°59.992
81m Triangular Mast S02°08.602 W59°00.033
Main Camp (Camp-1) S02°08.922 W59°00.195
Direct "Line Of Sight" Distances (Calculated from GPS):
ATTO Tall Tower to Walk-up Tower = 670m
ATTO Tall Tower to Triangular Mast = 630m
Walk-up Tower to Triangular Mast = 110m
Distances Along Roads and Trails (Measured by GPS):
Camp-1 to Tall Tower (Ramal 1) = 420m
Camp-1 to T2 (Ramal 1, Ramal 2, Trail A) = 840m
Compressors For Dryer / C4
Barbi House
81m Triangular Mast
C4
T2
C1
C3
C2
80m Walk-up Tower
Trail B
Aerosol Storage Container
Gas Storage
Trail A
Ramal 2
325m ATTO Tall Tower
Ramal 1
Power Cable Tall Tower Lights (Batteries Charge from Generators)
Vehicle Storage and Workshop
Camp-2
Power Cable - Camp-1 to Camp-2
Power Cable - T1 to T2
Power Cable - Aerosol Dryer
Power Cable - T1 to Camp-1
Camp-1 (Main ATTO Camp)
T1
Generators Location (as of 04-2016)
Ramal 1
200m
© 2016 Andrew Crozier
Road
Trail
Power Cable
Wooden Boardwalk
Container (Lab / Storage)
Building / Covered Structure
Transformer (T1 / T2)
GPS Point
LMA sites
EMBRAPA_AM010
T3 - DOE ARM ACRF
T0 - ATTO
CAREIRO DA VÁRZEA
MAIS 12
Camada sem título
ATTO Tall Tower
ATTO --> LMA center: 75km
XPOL @ Vila
Radar XPOL na Vila Rio Uatumã (?)
60km radius
ATTO --> XPOL@Vila: 35km
SIPAM Radar
100km radius
240km radius
WAIMIRI-ATROARI
CUNHÃ-SAPUCAIA
COATA LARANJAL
Manaus
JWD RWP CldRad GPS MP3000 Sodar Lidar